Cellular/Molecular

Dorsal BNST α_{2A}-Adrenergic Receptors Produce HCN-Dependent Excitatory Actions That Initiate Anxiogenic Behaviors

Nicholas A. Harris,[1,3] Austin T. Isaac,[1] Anne Günther,[7,9] Kevin Merkel,[1] James Melchior,[1,3] Michelle Xu,[1] Eghosa Eguakun,[1,2] Rafael Perez,[1,6] Brett P. Nabit,[1] Stephanie Flavin,[1,5] Ralf Gilsbach,[10] Brian Shonesy,[1,3] Lutz Hein,[10,11] Ted Abel,[12] Arnd Baumann,[8] Robert Matthews,[1] Samuel W. Centanni,[1,3] and Danny G. Winder[1,3,4,5,6,7]

[1]Vanderbilt Center for Addiction Research, [2]School for Science and Math at Vanderbilt, [3]Department of Molecular Physiology and Biophysics, [4]Vanderbilt J.F. Kennedy Center for Research on Human Development, [5]Vanderbilt Brain Institute, [6]Department of Pharmacology, [7]Department of Psychiatry and Behavioral Sciences, Vanderbilt University School of Medicine, Nashville, Tennessee 37232, [8]Department of Cellular Biophysics, Forschungszentrum Jülich, Germany, [9]Laboratory for Synaptic Molecules of Memory Persistence, RIKEN Center for Brain Science, Japan, [10]Institute of Experimental and Clinical Pharmacology and Toxicology, Faculty of Medicine, University of Freiburg, Freiburg 79104, Germany, [11]BIOSS Centre for Biological Signalling Studies, University of Freiburg, Freiburg 79104, Germany, and [12]Iowa Neuroscience Institute, Department of Molecular Physiology and Biophysics, Carver College of Medicine, University of Iowa, Iowa City, Iowa 52242

Stress is a precipitating agent in neuropsychiatric disease and initiates relapse to drug-seeking behavior in addicted patients. Targeting the stress system in protracted abstinence from drugs of abuse with anxiolytics may be an effective treatment modality for substance use disorders. α_{2A}-adrenergic receptors (α_{2A}-ARs) in extended amygdala structures play key roles in dampening stress responses. Contrary to early thinking, α_{2A}-ARs are expressed at non-noradrenergic sites in the brain. These non-noradrenergic α_{2A}-ARs play important roles in stress responses, but their cellular mechanisms of action are unclear. In humans, the α_{2A}-AR agonist guanfacine reduces overall craving and uncouples craving from stress, yet minimally affects relapse, potentially due to competing actions in the brain. Here, we show that heteroceptor α_{2A}-ARs postsynaptically enhance dorsal bed nucleus of the stria terminalis (dBNST) neuronal activity in mice of both sexes. This effect is mediated by hyperpolarization-activated cyclic nucleotide-gated cation channels because inhibition of these channels is necessary and sufficient for excitatory actions. Finally, this excitatory action is mimicked by clozapine-*N*-oxide activation of the G_i-coupled DREADD hM4Di in dBNST neurons and its activation elicits anxiety-like behavior in the elevated plus maze. Together, these data provide a framework for elucidating cell-specific actions of GPCR signaling and provide a potential mechanism whereby competing anxiogenic and anxiolytic actions of guanfacine may affect its clinical utility in the treatment of addiction.

Key words: alpha2a-adrenergic receptor; anxiety; bed nucleus of the stria terminalis; guanfacine; HCN channels; norepinephrine

Significance Statement

Stress affects the development of neuropsychiatric disorders including anxiety and addiction. Guanfacine is an α2A-adrenergic receptor (α2A-AR) agonist with actions in the bed nucleus of the stria terminalis (BNST) that produces antidepressant actions and uncouples stress from reward-related behaviors. Here, we show that guanfacine increases dorsal BNST neuronal activity through actions at postsynaptic α2A-ARs via a mechanism that involves hyperpolarization-activated cyclic nucleotide gated cation channels. This action is mimicked by activation of the designer receptor hM4Di expressed in the BNST, which also induces anxiety-like behaviors. Together, these data suggest that postsynaptic α2A-ARs in BNST have excitatory actions on BNST neurons and that these actions can be phenocopied by the so-called "inhibitory" DREADDs, suggesting that care must be taken regarding interpretation of data obtained with these tools.

Introduction

Stress contributes to the development of many neuropsychiatric disorders (Larzelere and Jones, 2008). Chronic stress exposure perpetuates maladaptive behaviors and leads to long-term physiological changes and autonomic dysregulation (Goeders, 2003; McEwen, 2004; Lampert et al., 2016; Sharma et al., 2016). Anxiety disorders can result from adverse life events and involve stress response generalization (Stein and Sareen, 2015; Miloyan et al., 2018). Anxiety disorder prevalence is as high as 22.8% (Kessler et al., 2005) and treatments are only partially effective with significant adverse effects (Griebel and Holmes, 2013). Further, anxiety and negative affect can occur during withdrawal and abstinence from drugs of abuse and alcohol (Sinha et al., 1999, 2011; Kassel et al., 2003; Heilig et al., 2010; Blaine et al., 2016). Therefore, anxiolytics may also be a viable treatment modality for addiction (Heilig and Egli, 2006; Bruijnzeel, 2017).

Agonists at the α_2-adrenergic receptor (α_2-AR) inhibit norepinephrine signaling to induce anxiolysis and decrease the stress response, among other actions (Buffalari et al., 2012; Ji et al., 2014; Strawn et al., 2017). For example, the α_{2A}-AR agonist guanfacine elicits antidepressant-like effects in the forced swim test (Mineur et al., 2015) and α_{2A}-AR KO mice show elevated baseline anxiety- and depressive-like behaviors (Schramm et al., 2001; Lähdesmäki et al., 2002). Further, in rodent models of addiction, α_2-AR agonists block stress-induced reinstatement of drug-seeking behaviors (Erb et al., 2000; Shaham et al., 2000; Highfield et al., 2001; Mantsch et al., 2010).

Direct administration of α_2-AR agonists to the bed nucleus of the stria terminalis (BNST) inhibits both stress-induced anxiety-like behavior (Schweimer et al., 2005) and drug-seeking behavior (Delfs et al., 2000; Wang et al., 2001). As part of the extended amygdala, the BNST functions in stress–reward integration and has been implicated in both anxiety disorders (Adhikari, 2014) and reinstatement of drug-seeking behaviors (Koob, 2009). Noradrenergic input to the BNST via the ventral noradrenergic bundle is critical for stress-induced reinstatement of drug-seeking behavior (Shalev et al., 2001; Wang et al., 2001). Presynaptic α_{2A}-ARs inhibit norepinephrine release in the BNST and may inhibit stress effects in this manner (Park et al., 2009). However, heteroceptor α_{2A}-ARs regulate glutamatergic transmission in the BNST in an input-specific manner, inhibiting parabrachial nucleus (PBN) but not basolateral amygdala (BLA) afferents (Shields et al., 2009; Flavin et al., 2014). Immunoelectron microscopy showed that BNST α_{2A}-ARs are expressed in both presynaptic specializations (i.e., asymmetric/symmetric axon terminals) and postsynaptic specializations (dendrites, spines, soma) (Flavin et al., 2014). The relationship among α_{2A}-AR populations and their contributions to behavior remain unknown.

α_{2A}-ARs are G_i-coupled GPCRs and are thus classically thought to impair neuronal signaling. However, stimulatory effects on neuronal activity have been reported for this and other G_i-GPCRs (Federman et al., 1992; Andrade, 1993; Winder and Conn, 1993). Guanfacine upregulates expression of the immediate early gene cfos, an indirect marker of neuronal activity, in the BNST and other regions (Savchenko and Boughter, 2011). In the prefrontal cortex, α_{2A}-AR activation has been shown to decrease the open probability of hyperpolarization-activated and cyclic nucleotide-gated cation (HCN) channels localized to the dendritic neck separating the dendritic spine from the dendrite and the soma to increase fidelity of synaptic current transmission and pyramidal neuron network activity (Wang et al., 2007).

Here, we show that guanfacine-induced excitatory actions within the dorsal BNST (dBNST) occur via activation of postsynaptic α_{2A}-ARs using convergent techniques including transgenic mouse models targeting the α_{2A}-AR, RNA *in situ* hybridization, *ex vivo* incubation, and chemogenetics. The mechanism underlying this effect is shown to involve pacemaker channels containing HCN2 subunits, which are anatomically and functionally colocalized in dBNST neurons expressing α_{2A}-ARs and are both necessary and sufficient for guanfacine-induced excitatory actions. Finally, at the behavioral level, postsynaptic α_{2A}-AR activity within the BNST is shown to compete with the overall anxiolytic actions of systemic guanfacine application because the introduction and expression of an unrelated inhibitory chemogenetic receptor, hM4Di, elicited activity-enhancing effects and led to anxiety-like behavior in transduced mice.

Materials and Methods

Animals. Male and female mice of at least 8 weeks of age were used throughout this study. Male C57BL/6J mice (RRID:IMSR_JAX:000664; The Jackson Laboratory;) were delivered at 7 weeks of age and acclimated for 1 week before use. Multiple lines of α_{2A}-AR transgenic mice were bred in-house from homozygote ($TG^-\ WT^{-/-} \times TG^+\ WT^{-/-}$ where TG = *Dbh-Adra2a* and WT = *Adra2a*) or heterozygote breeders ($TG^-\ WT^{+/-} \times TG^+\ WT^{+/-}$) and genotyped as described previously (Gilsbach et al., 2009). WT controls were negative for *Dbh-Adra2a* and homozygous positive for WT *Adra2a*. *cfos-eGFP* mice (RRID:IMSR_JAX:014135; The Jackson Laboratory) were bred in-house and genotyped as described previously (Barth et al., 2004). Thy1-COP4 mice (line 9) were bred in-house on a homozygote background (RRID:IMSR_JAX:007615; The Jackson Laboratory strain 007615) (Arenkiel et al., 2007). For *Adra2a* KO, *Dbh-Adra2a*, *Adra2a* WT, *cfos-eGFP*, and Thy1-COP4 mouse lines, mice of both sexes were used to minimize the total number of animals. No sex differences were apparent, so each group is compiled into a single value representative of both sexes. Each mouse line was maintained on a C57BL/6J background and back-crossed as needed. All mice were group housed with two to five animals per cage and maintained on 12 h light/dark cycle (lights on at 0600 h) under controlled temperature (20–25°C) and humidity (30–50%) levels. Mice were given access to food and water *ad libitum*. All treatments and interventions were approved by the Vanderbilt Animal Care and Use Committee.

Reagents. All *in vivo* injections were done with sterile saline as vehicle (0.9% sodium chloride; Hospira). Guanfacine hydrochloride (#1030, >99%) and atipamezole hydrochloride (#2937, >99%) were obtained from Fisher Scientific and diluted in sterile saline (guanfacine: 1 mg/10 ml = 0.35 mM) or deionized (di)H_2O as stock solution (both: 10 mM). ZD7288 was obtained from R&D Systems (#1000, >99%) and diluted in diH_2O as stock solution (10 mM). Clonidine (#0690, >99%) and UK-14304 (#2466, >99%) were obtained from Tocris Bioscience and diluted in diH_2O as stock solution (10 mM). Clozapine-*N*-oxide (CNO) was obtained from Sigma-Aldrich (#C0832, >98%;) and diluted in sterile saline (3 mg/10 ml = 0.88 mM). Metacam was obtained

Received April 15, 2018; revised Aug. 15, 2018; accepted Aug. 20, 2018.

Author contributions: N.A.H. wrote the first draft of the paper; N.A.H., A.T.I., A.G., K.R.M., J.R.M., M.A.X., E.J.E., R.P., B.P.N., S.A.F., R.G., B.C.S., L.H., T.A., A.B., R.T.M., S.W.C., and D.G.W. edited the paper; N.A.H., S.W.C., and D.G.W. designed research; N.A.H., A.T.I., K.R.M., J.R.M., M.A.X., E.J.E., R.P., B.P.N., S.A.F., and R.T.M. performed research; A.G., R.G., B.C.S., L.H., T.A., and A.B. contributed unpublished reagents/analytic tools; N.A.H., A.T.I., K.R.M., J.R.M., M.A.X., E.J.E., and S.A.F. analyzed data; N.A.H. and D.G.W. wrote the paper.

This work was supported by National Institutes of Health (Grant R01DA042475 to D.G.W., Grant F30DA042501 to N.A.H., and Grant T32GM07347 to N.A.H.). L.H. was supported by the BIOSS Centre for Biological Signalling Studies. Imaging and image data analyses were performed in part through the use of the Vanderbilt University School of Medicine Cell Imaging Shared Resource (supported by National Institutes of Health Grants CA68485, DK20593, DK58404, DK59637, and EY08126). We thank Elana Milano for technical assistance.

The authors declare no competing financial interests.

Correspondence should be addressed to Dr. Danny G. Winder, Vanderbilt Center for Addiction Research, 23rd and Pierce Ave. S., Room 865A, Vanderbilt University School of Medicine, Nashville, TN 37232-0615. E-mail: danny.winder@vanderbilt.edu.

DOI:10.1523/JNEUROSCI.0963-18.2018

 0270-6474/18/388923-21$15.00/0

from Patterson Veterinary (#07-845-6986) and diluted in sterile saline (2.5 mg/10 ml). Primary antibodies were used at 1:1000 dilution and included rabbit anti-cfos (Millipore; abe457; RRID:AB_2631318), mouse anti-NeuN (Millipore mab377 clone A60; RRID:AB_2298772), and chicken anti-GFP (Abcam; ab13970; RRID:AB_300798). Secondary antibodies (Jackson ImmunoResearch), including Cy2 donkey anti-rabbit (711-225-152; RRID:AB_2340612), Cy3 donkey anti-mouse (715-165-150; RRID:AB_2340813), Cy2 donkey anti-chicken (703-225-155; RRID:AB_2340370), and Cy5 donkey anti-rabbit (711-175-152; RRID:AB_2340607), were diluted in equal volumes of sterile H_2O and glycerol and used at a final dilution of 1:400. Adeno-associated viral (AAV) vectors were used as received and included AAV5-CaMKIIα-hM4Di:mCherry (AAV5-hM4Di; UNC Viral Vector Core), AAV5-CaMKIIα-mCherry (AAV5-mCherry; UNC Viral Vector Core), AAV9-CMV-eGFP (AAV9-GFP; UNC Viral Vector Core), and AAV5-hSyn-GCaMP6f (AAV5-GCaMP6f; Addgene). AAV5-GCaMP6f and AAV5-hM4Di or AAV5-mCherry were mixed in equal volumes immediately before injection. In addition, AAV9-hU6-shHCN1-shHCN2-CaMKIIα-eGFP (AAV9-shHCN1/2) was produced by standard protocol, purified with an iodixanol density gradient, and filtered and concentrated in PBS using centrifugal filter cartridges. Final titers were determined by qPCR and specificity and efficiency were tested by qPCR and Western blot in cell culture and hippocampal tissue (data not shown).

Fast-scan cyclic voltammetry. Slice preparation (Wills et al., 2012; Flavin et al., 2014) and voltammetry were performed as described previously (Melchior et al., 2015; Melchior and Jones, 2017). Briefly, mice were anesthetized with isoflurane, decapitated, and coronal slices (300 μm thick) containing BNST were prepared in ice-cold, oxygenated artificial CSF (ACSF) consisting of the following (in mM): 126 NaCl, 2.5 KCl, 1.2 NaH_2PO_4, 2.4 $CaCl_2$, 1.2 $MgCl_2$, 25 $NaHCO_3$, 11 glucose, and 0.4 L-ascorbic acid, pH adjusted to 7.4. Slices were allowed to recover in oxygenated ACSF at room temperature for 1 h and then transferred to a recording chamber through which 32°C oxygenated ACSF was perfused at a rate of 2 ml/min. A carbon fiber electrode (150 μm length) was placed into the ventral BNST ~200 μm ventral to the anterior commissure. Extracellular catecholamine signals were monitored at the carbon fiber electrode every 100 ms using fast scan cyclic voltammetry (Wightman et al., 1988) with an applied waveform ranging from −0.4 to 1.2 V vs Ag/AgCl reference at a rate of 400 V/s. A bipolar stimulating electrode was placed on the surface of the slice ~150 μM from the carbon fiber recording electrode. Catecholamine release was evoked by an electrical pulse (550 μA, 4 ms duration) applied as a 20-pulse stimulation train (20 Hz) once every 10 min. Baseline recordings were obtained until the catecholamine release amplitude was stable (<10% variation across three recordings). Subsequently, guanfacine hydrochloride (10 μM) was applied to the slice buffer and recordings continued for 60 min. For each slice, a single baseline release value was determined by averaging the final two baseline recordings and the drug effect was determined by averaging the final two recordings in drug and presented as the percentage change from the baseline value.

Fluorescent immunohistochemistry. Mice were handled for 5 d as described previously (Olsen and Winder, 2010). After removal from the colony, mice recovered for at least 1 h in a Med Associates sound-attenuating chamber and injected intraperitoneally with guanfacine (1 mg/kg), CNO (3 mg/kg), guanfacine and CNO, or saline 90 min before perfusion. Under isoflurane anesthesia, mice were transcardially perfused with 10 ml of ice-cold PBS followed by 20 ml of 4% paraformaldehyde (PFA) in PBS. Extracted brains were submerged in 4% PFA for 24 h at 4°C and cryoprotected in 30% sucrose in PBS for a minimum of 2 d. Coronal sections were cut on a cryostat (Leica, CM3050S) in optimal cutting temperature (OCT) solution (VWR) at a thickness of 40 μm and stored in PBS at 4°C until immunological staining.

For cfos staining, coronal sections were washed with PBS (4 × 10 min), permeabilized with 0.5% Triton X-100 in PBS (1 h), and blocked with 5% normal donkey serum (NDS) and 0.5% bovine serum albumin (BSA) for 1 h at room temperature (RT). Primary antibodies were applied in blocking solution and slices were incubated in primary antibody (rabbit anti-cfos, mouse anti-NeuN, chicken anti-GFP) for 24 h at RT, washed in PBS (4 × 10 min), and incubated in combinations of secondary antibodies (Cy2 donkey anti-rabbit, Cy2 donkey anti-chicken, Cy3 donkey anti-mouse, Cy5 donkey anti-rabbit) in 0.1% Triton X-100 in PBS for 24 h at 4°C. Slices were stained with DAPI (1:10,000, Life Technologies; D3571), washed in PBS (4 × 10 min), mounted on Fisher Plus slides (Fisher Scientific), and coverslipped with PolyAquamount (Polysciences) when dry. Slight modifications were used to visualize cfos-eGFP transgene expression. In this case, a modified blocking solution (10% NDS and 0.1% Triton X-1000 in PBS), a shorter time of permeabilization (30 min), and longer primary antibody incubation (48 h at 4°C) were used.

All images were obtained with a Zeiss 880 scanning confocal microscope using either a 20×/0.80 numerical aperture (NA Plan-Apochromat, 40×/1.30 NA C Plan-Apochromat oil, or 63×/1.40 NA Plan-Apochromat Oil objective lens. Excitation/emission wavelengths (nm) for each fluorophore were 405.0/461.5 (DAPI), 448/521.5 (Cy2, GFP), 561.0/610.8 (Cy3, mCherry), and 633.0/701.8 (Cy5). The same acquisition parameters and alterations to brightness and contrast in ImageJ were used across all images within an experiment. Cells were manually counted using ImageJ by a blinded reviewer. No overt differences were observed between subnuclei of the dorsal BNST, so all numbers are reported as a single averaged value for each dBNST and then averaged for each animal.

RNA in situ *hybridization*. A variant of fluorescence *in situ* hybridization (FISH) known as RNAScope (Advanced Cell Diagnostics) was used to visualize RNA transcripts in fresh-frozen BNST coronal sections. The procedure was performed as described previously (Ghamari-Langroudi et al., 2015). RNAScope cDNA probes and detection kits were purchased from Advanced Cell Diagnostics and used according to the company's online protocols. All probes were generated against *Mus musculus*-specific transcripts and included *Adra2a* (#425341, channel C1, target region 2345–3381, accession number NM_007417.4), *Fos* (#316921-C2, C2, 407–1427, NM_010234.2), *Hcn1* (#423651-C2, C2, 2158–3777, NM_010408.3), *Hcn2* (#427008-C2, C2, 687–1878, NM_008226.2), *Prkcd* (#441791-C3, C3, 334–1237, NM_011103.3), *Penk* (#318761-C2, C2, 106–1332, NM_0001002927.2), *Calb2* (#313641-C2, C2, 147–1265, NM_007586.1), *Crf* (#316091-C2, C2, 20–1262, NM_205769.2), and *Npy* (#313321-C3, C3, 28–548, NM_023456.2).

Mice used to monitor *Fos* transcript colocalization were handled and injected as described above. For expression analysis of HCN subunits, mice were equivalently handled but never injected. Brains were extracted under isoflurane anesthesia, submerged in oxygenated (5% CO_2/95% O_2) ice-cold ACSF containing the following (in mM): 124 NaCl, 4.4 KCl, 2.5 $CaCl_2$, 1.3 $MgSO_4$, 1 NaH_2PO_4, 10 glucose, and 26 $NaHCO_3$ and frozen in OCT using Super Friendly Freeze-It Spray (Fisher Scientific). Embedded brains were stored in dry ice and then at −80°C until further use. Then, 16 μm sections were cut on a cryostat (Leica, CM3000) and transferred to Fisher plus slides (Fisher Scientific) chilled with dry ice and stored at −80°C. Samples were fixed in 4% PFA at 4°C for 15 min, dehydrated in an ethanol dilution series (50%, 70%, 100% × 2 for 5 min each), and air-dried for 5 min. A hydrophobic barrier was drawn around each slice with a PAP barrier pen before incubation with Advanced Cell Diagnostics's pretreatment 4 solution (30 min at 40°C), then RNAScope probes (2 h at 40°C), then Amp 1-FL solution (30 min at 40°C), Amp 2-FL solution (15 min at 40°C), Amp 3-FL solution (30 min at 40°C), and Amp 4-FL ALT B solution (15 min at 40°C) with 2 min of washing in wash buffer (2×) in between each step. Slides were counterstained with 1:10,000 DAPI for 30 s at RT before coverslipping with Aqua PolyMount. A minimum of two slices (one slice per slide) were used from each animal: one experimental group and one negative control (three probe sets for bacterial DapB mRNA in channels 1–3 (Advanced Cell Diagnostics). Slices from each mouse were examined with different probes.

Sections were imaged with a Zeiss 880 scanning confocal microscope using either a Plan-Apochromat 20×/0.80 NA or 63×/1.40 oil lens. *Z* stacks were done on all high-magnification images such that the depth of the tissue was covered in 8 images (1 image per 2 μm). The BNST was visualized at 10× magnification (10×/0.50 NA lens) and then three 63× images were obtained to cover the dorsal, medial, and lateral components of the dorsal BNST. Each image was quantified individually, but because no differences were observed between the three subregions, the counts

were compiled into a single average value for each dorsal BNST and then averaged for each animal. *Z* stacks were transformed into single layer images using ImageJ Z-project (maximum intensity). Transcripts were readily identified as small, round, and distinct dots over and surrounding DAPI-labeled nuclei (see Figs. 2*C*, 6*A* for example images). Negative control images were used to determine brightness and contrast parameters that minimized observation of the bacterial transcripts and autofluorescence, which were then used for experimental images. Dots per cell were manually counted across all images by a blinded reviewer. To determine the threshold for transcript positivity in experimental slices, the numbers of dots per cell were counted in negative control images and the threshold for positivity was calculated as the mean number of dots per cell plus 3 SDs such that 99.7% of negative control cells were below this threshold.

Ex vivo *preincubation*. Brain slices were obtained as described above. *cfos-eGFP* mice were handled and injected as described above. After preparation, slices were sequentially transferred to one of four holding chambers in oxygenated ACSF at 28°C and allowed to recover for 1 h. In the first preincubation experiment, guanfacine (1 μM), atipamezole (1 μM), both guanfacine and atipamezole, or vehicle was added to the holding chamber from stock solutions. In the second preincubation experiment, guanfacine (1 μM), clonidine (10 μM), UK-14304 (10 μM), or vehicle was equivalently added. After 60 min of incubation, slices were fixed in 4% PFA for 30 min at RT before being transferred to 4°C for 24 h. Slices were then transferred to PBS and maintained at 4°C until further use.

The Brain Blocking of Lipids and Aldehyde Quenching (BLAQ) procedure was used as described previously (Kupferschmidt et al., 2015). Sections were washed for 1 h in PBST (0.2% Triton X-100 in PBS), rinsed twice for 1 min in diH_2O, quenched in freshly prepared sodium borohydride ($NaBH_4$; 5 mg/ml = 132 mM in diH_2O; Sigma-Aldrich, #213462, 99%), rinsed again in diH_2O (2× for 1 min), incubated twice for 15 min in Sudan Black B solution (0.2% in 70% ethanol), washed twice for 30 min in PBS, and incubated for 4 h in 5% NDS in PBST. Slices were incubated in primary antibody (chicken anti-GFP, mouse anti-NeuN) for 72 h at 4°C, washed 4 times in PBST for a total of 24 h at 4°C, and then incubated in secondary antibody (Cy2 donkey anti-chicken, Cy3 donkey-anti mouse) for 48 h at 4°C. Finally, slices were washed 4 times in PBST for a total of 24 h at 4°C, washed in PBS for 1 h at RT, and then mounted on Fisher Plus slides and coverslipped with Poly AquaMount when dry. Images were obtained with a Zeiss 880 scanning confocal microscope using a 63×/1.40 NA Plan-Apochromat Oil objective lens and processed as described above for fluorescent immunohistochemistry.

Microinjection surgeries. Mice were anesthetized with isoflurane (initial dose = 3%; maintenance dose = 1.5%) and injected intracranially with recombinant AAV constructs. A targeted microinjection of the viruses (200–300 nl) was made into the BNST (AP: 0.14, ML: ±0.88, DV: −4.24) (Paxinos and Franklin, 2004) at a 15.03° angle. All injections were bilateral except for the dual AAV5-GCaMP6f and AAV5-hM4Di or AAV5-mCherry injections, which were unilateral on the right side. Mice were treated with 5 mg/kg injections of ketoprofen or metacam for 48 h following surgery. All mice except the GCaMP6f-injected animals were killed 3 weeks after surgery for anatomical analysis. GCaMP6f-injected animals underwent implantation of optical fibers at least 3 weeks after viral injection followed by subsequent behavioral analysis.

Current-clamp recordings Whole-cell current-clamp recordings were performed as described previously (Kash and Winder, 2006; Silberman et al., 2013; Flavin et al., 2014). For current-clamp recordings, electrodes (3.0–5.0 MΩ) were filled with the following (in mM): 135 K^+-gluconate, 5 NaCl, 10 HEPES, 0.6 EGTA, and 4 Na_2GTP, pH 7.2–7.4, osmolarity 290–295.

cfos-eGFP mice were handled and injecte, and brain slices were prepared as described above. After 1 h of recovery in heated (28°C) oxygenated ACSF, slices were transferred to a second heated holding chamber with either unaltered ACSF or ACSF containing 10 μM ZD7288 for 1 h before recording. In the recording chamber, slices were continuously perfused with oxygenated and heated (28°C) ACSF at a rate of 1–2 ml/min. Picrotoxin (25 μM) was used to isolate excitatory transmission. cfos-eGFP$^+$ cells were identified using a mercury lamp light source, EN-GFP filter cube, and infrared video microscopy (all Olympus) for patching.

After achieving whole-cell configuration, cells were equilibrated for 2–5 min before recording. Postsynaptic parameters were monitored continuously during the experiments and cells were excluded if the access resistance (R_a) changed by >20% in either direction. Current-clamp profiles, defined here as the whole-cell membrane potential changes that occur in response to positive and negative current injections, were obtained at resting membrane potential and consisted of current injections ranging from −200 pA to +200 pA with a step of 20 pA per injection. Once a current-clamp profile was obtained, spontaneous EPSPs (sEPSPs) were recorded for 5 min. After 1 h of recording, slices were transferred to 4% PFA and processed for BLAQ as described above. Current-clamp recordings from small hairpin RNA (shRNA)-injected C57BL/6J mice were similarly performed except that these mice were never injected and slices were not incubated with ZD7288.

All whole-cell data were recorded with Clampex 10.2 and analyzed with pClamp 10.2 (Molecular Devices). Resting membrane potential was calculated before current injection. Hyperpolarization sag was calculated as the difference between the initial maximal negative membrane potential and the steady-state current after negative current injection. The time constant of I_h activation (τ) was calculated as the time to reach 1–1/e (63.2%) of steady-state potential from maximal negative potential. sEPSP measurements were analyzed with pClamp 10.2 using the "event detection" template created for each trace individually to obtain amplitude and frequency of sEPSP events.

Field potential recordings. Thy1-COP4 mice were used for optical field potential recordings. Slices were prepared as described above. Picrotoxin (25 μM) was used to isolate excitatory transmission. Light stimulation was driven from a T-Cube LED Driver (LEDD1B; Thorlabs) passed through an EN-GFP filter cube (Olympus) to produce blue wavelength light. Light stimuli were ~2 ms in duration and occurred every 10 s. Optically evoked field potentials were observed as negative deflections with dual N1 (oN1) and N2 (oN2) components. The oN2 component was kynurenic acid sensitive, whereas the oN1 component was kynurenic acid insensitive (data not shown) and are thus analogous to the fiber volley potential N1 and the synaptic potential N2 recorded as part of electrically evoked field potentials within the BNST (Weitlauf et al., 2004; Egli et al., 2005; Conrad et al., 2012). Data were excluded if the oN1 changed by >20% during the experiment. All field potential data were collected using Clampex 10.2 (Molecular Devices) and analyzed via Clampfit 10.2 (Molecular Devices) as described previously (Shields et al., 2009; Flavin et al., 2014). Plotted time courses are represented as 1 min averages relative to baseline (0–5 min for guanfacine, 0–10 min for ZD7288).

Stereotaxic chronic optical fiber implantation. Three weeks after injection of AAV5-GCaMP6f and AAV5-hM4Di or AAV5-mCherry, mice were anesthetized with isoflurane and underwent stereotaxic surgery for optical fiber implantation. The optical fiber implant was constructed from a 0.22 NA, 300 μm core multimode fiber (Thorlabs) placed inside a mounting ferrule with Epo-Tek general room temperature cure epoxy (Fiber Optic Center) and cured at 45°C overnight. The fiber was cut on one end with an Ideal DualScribe Wedge Tip Carbide Scribe (Fiber Optic Center) and polished using a Ferrule Polishing Disc (Thorlabs) on progressively finer aluminum oxide lapping sheets (5, 3, 1, 0.1 μm). Both sides were visually inspected for aberrations and were not used if deemed unsatisfactory. Briefly, after exposure of the skull, gel etchant was used to clean the skull, a screw was placed rostral to the craniotomy hole, the implant was slowly lowered through the previously made craniotomy hole into the BNST at a 15.03° angle, Optibond FL Primer was applied around the implant, Optibond FL adhesive was applied and cured, and Herculite Unidose Enamel was applied and cured. After surgery, mice were given Diet Gel as well as subcutaneous injections of ketoprofen or metacam and 1 ml of saline for 72 h. A minimum of 2 weeks of recovery was used before mice underwent behavioral and fiber photometric testing.

In vivo *fiber photometry apparatus.* The fiber photometry measurements in this study were performed by the ChiSquare 2–202 dual-probe system (ChiSquare Biomaging). Briefly, blue light from a 473 nm

picosecond-pulsed laser (at 50 MHz; pulse width ~80 ps FWHM) was delivered to the sample through a single mode fiber. Fluorescence emission from the tissue was collected by a multimode fiber. The single mode and multimode fibers were arranged side by side (Cui et al., 2013) in a ferrule connected to a detachable multimode fiber implant. The emitted photons collected through the multimode fiber passed through a bandpass filter (FF01-550/88; Semrock) to a single-photon detector. Photons were recorded by the time-correlated single photon counting module (SPC-130EM; Becker and Hickl) in the ChiSquare 2–202 dual-probe system. A fluorescence intensity trace was obtained by plotting the number of photons recorded in 20 ms intervals against time. Fluorescence decay kinetics were used to confirm *in vivo* GcaMP6f expression.

Elevated plus maze (EPM) behavior and fiber photometric recordings. All behavior experiments were performed during the light phase. Mice were handled and injected as described above before and during behavioral experiments. In addition, the last 2 d of handling involved transport to the laboratory and habituation to fiber photometry manipulations, including cleaning of implants with ethanol and lens paper, and recording fiber photometry signal via a 200 μm core 0.5 NA FC/PC to 1.25 mm ferrule patch cable (Thorlabs) connected to the implant. Before behavioral testing, mice were injected with CNO or saline 2 h before recording a baseline for 2 min. This baseline recording occurred in the home cage after acclimation to connection with the patch cord for 5 min. Then mice were transferred to the EPM for 5 min. This apparatus is elevated 55 cm above the floor and consists of four arms (30.5 × 6.5 cm), 2 open and 2 closed (16 cm wall height), with a 5 × 5 cm open center zone. Lighting was set to ~60–70 lux in the open arm and 10–20 lux in the closed arm. Mice were visualized, recorded, and tracked by a camera using AnyMaze software (Stoelting). Fiber photometry recordings began upon receipt of a transistor-transistor logic pulse from AnyMaze; therefore, the behavior and fiber photometry signal were precisely time locked. Raw photon count was converted to $\Delta F/F_0$ using a segmented normalization procedure with a bin of 4 s. Ca^{2+} transients were identified using a Savitsky–Golay filter and empirically determined kinetic parameters using the mLspike algorithm (Deneux et al., 2016). The frequency of Ca^{2+} transients was calculated for both recordings. In addition, the transients were temporally aligned with mouse location to yield open and closed arm frequencies.

Experimental design and statistical analysis. The number of animals to be used in each experiment were predetermined based on analyses of similar experiments in the literature and supplemented as needed based on observed effect sizes (Savchenko and Boughter, 2011; Silberman et al., 2013; Flavin et al., 2014; Ghamari-Langroudi et al., 2015; Kupferschmidt et al., 2015, 2017; Holleran et al., 2016). For experiments involving male and female mice, a minimum of three mice of both sexes was used to allow for sex difference statistical comparisons to be performed. All data are represented as mean ± SEM. All statistics were run using Prism 7 (GraphPad). Differences between groups were assessed using *t* tests, one-way ANOVAs, and two-way ANOVAs, with significance set at $\alpha = 0.05$. When significant main effects were obtained using ANOVA tests, appropriate *post hoc* comparisons between groups were performed.

Results

Guanfacine induces cfos expression in the dBNST dependent on the expression of α_{2A}-ARs in non-noradrenergic neurons

To determine what populations of α_{2A}-ARs contribute to guanfacine-induced cfos expression in the dBNST, we compared effects in WT mice and two transgenic mouse strains targeting the *Adra2a* gene. The transgenic genotypes were a complete α_{2A}-AR KO (*Adra2a*$^{-/-}$) and a transgenic rescue reintroducing the *Adra2a* gene under the control of the dopamine β-hydroxylase promoter into an *Adra2a*$^{-/-}$ background (Gilsbach et al., 2009). The rescue results in the expression of α_{2A}-AR exclusively in noradrenergic neurons. These lines allow for the differentiation of autoreceptor and heteroceptor mechanisms of α_{2A}-AR physiology and pharmacology (Fig. 1*A*,*B*). We validated the functional autoreceptor expression pattern of α_{2A}-ARs within these mouse lines using fast scan cyclic voltammetry. To do this, we measured extracellular catecholamine levels in the ventral BNST after local electrical stimulation and determined autoreceptor α_{2A}-AR function by measuring the effects of guanfacine (10 μM) on catecholamine levels (Fig. 1*C*). In WT mice, guanfacine decreased stimulus-evoked catecholamine transients to 69.2 ± 3.9% of baseline levels (baseline: 10–30 min; guanfacine: 70–90 min; paired *t* test, $p = 0.002$; Fig. 1*D*, blue). This effect was absent in full *Adra2a*$^{-/-}$ mice (109.1 ± 3.1%; $p = 0.12$; Fig. 1*D*, red), but rescued in heteroceptor-specific *Adra2a*$^{-/-}$ mice (76.5 ± 5.1%; $p = 0.01$; Fig. 1*D*, green). A repeated-measures two-way ANOVA revealed a significant effect of time ($F_{(9,126)} = 8.01$, $p < 0.0001$), genotype ($F_{(2,14)} = 19.99$, $p < 0.0001$), and subject ($F_{(14,126)} = 2.93$, $p = 0.0007$), as well as an interaction between time and genotype ($F_{(18,126)} = 4.81$, $p < 0.0001$) on measured extracellular catecholamine transient levels. Holm–Sidak's multiple-comparisons test was performed *post hoc* between the genotypes at all time points. Extracellular catecholamine transient levels were lower in WT than full *Adra2a*$^{-/-}$ mice at all time points after 50 min (0 min, $p = 0.47$; 10 min, $p = 0.84$; 20 min, $p = 0.92$; 30 min, $p = 0.92$; 40 min, $p = 0.07$; 50 min, $p = 0.004$; 60 min, $p < 0.0001$; 70 min, $p < 0.0001$; 80 min, $p < 0.0001$; 90 min, $p < 0.0001$) and in heteroceptor-specific relative to full *Adra2a*$^{-/-}$ mice after 60 min (0 min, $p = 0.90$; 10 min, $p = 0.84$; 20 min, $p = 0.92$; 30 min, $p = 0.92$; 40 min, $p = 0.36$; 50 min, $p = 0.57$; 60 min, $p = 0.03$; 70 min, $p = 0.01$; 80 min, $p < 0.0001$; 90 min, $p < 0.0001$). Between 50 and 70 min, evoked catecholamine transients in heteroceptor-specific *Adra2a*$^{-/-}$ mice were significantly higher than WT littermates (0 min, $p = 0.47$; 10 min, $p = 0.998$; 20 min, $p = 0.92$; 30 min, $p = 0.92$; 40 min, $p = 0.36$; 50 min, $p = 0.02$; 60 min, $p = 0.004$; 70 min, $p = 0.02$; 80 min, $p = 0.31$; 90 min, $p = 0.23$). To determine the overall guanfacine effect, a one-way ANOVA was performed at the final time points (70–90 min) and revealed significant differences among the three genotypes ($F_{(2,12)} = 27.94$, $p < 0.0001$; Fig. 1*E*). Holm–Sidak's multiple-comparisons test was performed *post hoc* between all genotypes and showed there to be significant differences between WT and full ($p < 0.0001$) but not heteroceptor-specific ($p = 0.38$) *Adra2a*$^{-/-}$ mice. Further, there was a significant difference between full and heteroceptor-specific ($p < 0.0001$) KO mice.

We next evaluated neuronal cfos expression 90 min after saline or guanfacine (1 mg/kg) injections (Fig. 1*F*,*G*). A two-way ANOVA revealed a significant interaction between treatment and genotype ($F_{(2,105)} = 11.62$, $p < 0.0001$), no significant effect of genotype alone ($F_{(2,105)} = 0.88$, $p = 0.42$), and a significant effect of treatment alone ($F_{(1,105)} = 5.24$, $p = 0.02$) (Fig. 1*H*). A Holm–Sidak multiple-comparisons test was performed *post hoc* between all groups. Guanfacine-injected animals showed increased cfos levels in WT animals (WT saline: 4.4 ± 0.9%; WT guanfacine: 14.2 ± 1.4%; $p = 0.0004$), but not in full α_{2A}-AR KO (KO saline: 13.5 ± 1.3%; KO guanfacine: 9.0 ± 0.6%; $p = 0.19$) or heteroceptor-specific α_{2A}-AR KO animals (KO+TG saline: 8.8 ± 1.6%; KO+TG guanfacine: 11.7 ± 1.4%; $p = 0.58$). When injected with saline, α_{2A}-AR KO mice show increased cfos expression relative to WT controls ($p = 0.0004$), whereas there was no difference between heteroceptor-specific α_{2A}-AR KO mice and WT controls ($p = 0.33$) or full α_{2A}-AR KO mice ($p = 0.07$). Together, these data show that guanfacine-induced cfos expression is only observed in WT animals and an elevated cfos response to saline occurs in α_{2A}-AR KO mice.

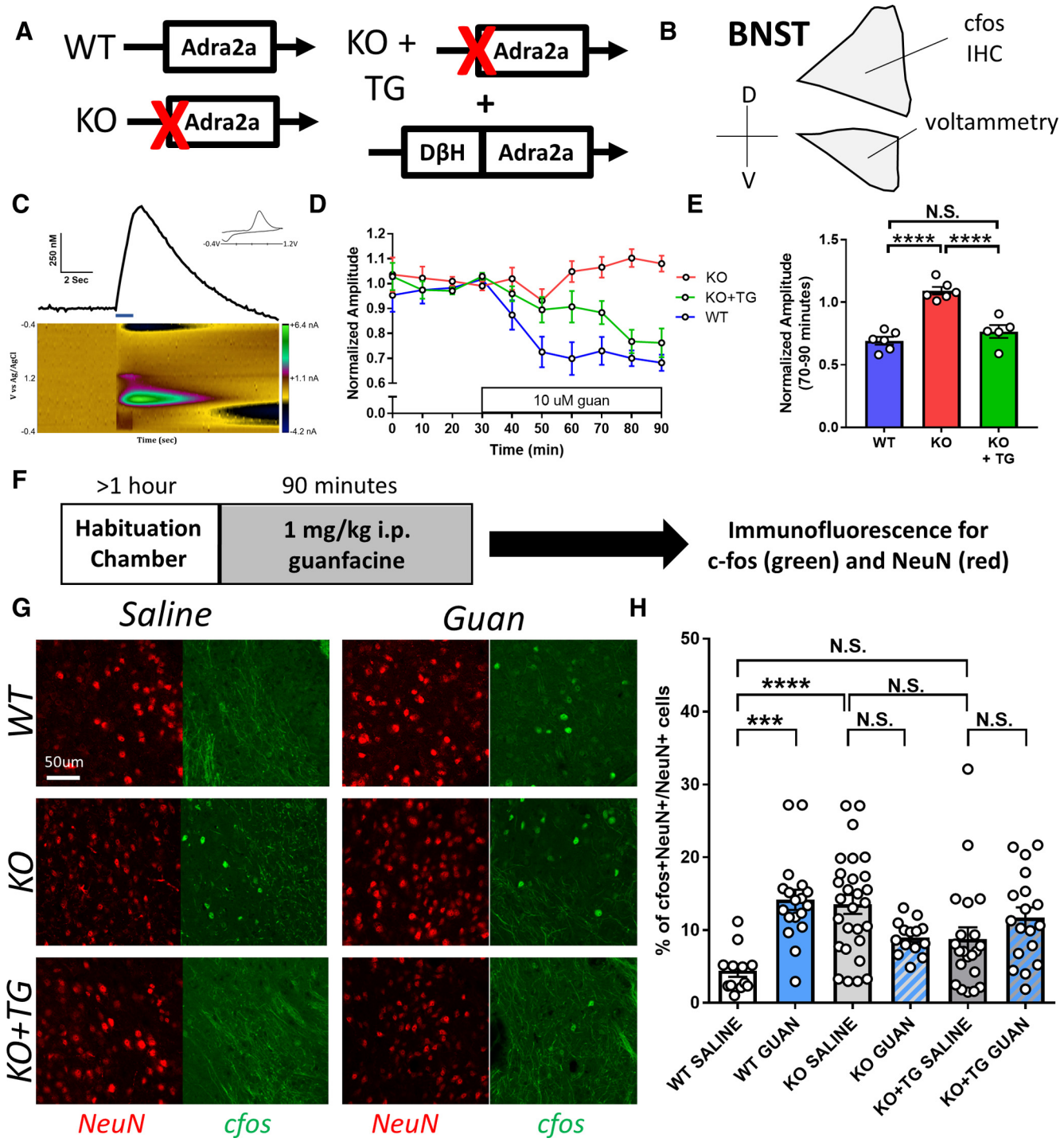

Figure 1. Guanfacine-induced cfos expression in the dBNST is dependent on the expression of α_{2A}-ARs in non-noradrenergic neurons. ***A***, Schematic showing genetic differences between the three different *Adra2a* mouse lines. ***B***, Anatomical diagram showing location of immunohistochemistry and voltammetry experiments within the BNST. ***C***, Representative fast scan cyclic voltammetry trace showing catecholamine measurement after electrical stimulation in ventral BNST. ***D***, Time course of guanfacine (10 μM) application on amplitude of extracellular catecholamine in the ventral BNST. WT and heteroceptor-specific *Adra2a*$^{-/-}$ mice show a decrease after guanfacine (70–90 min) application relative to baseline (10–30 min; WT: 69.2 ± 3.9%, $p = 0.002$; KO+TG: 76.5 ± 5.1%, $p = 0.01$) while full *Adra2a*$^{-/-}$ do not (109.1 ± 3.1%, $p = 0.12$). Two-way ANOVA: time effect $F_{(9,126)} = 8.01$, $p < 0.0001$, genotype effect $F_{(2,14)} = 19.99$, $p < 0.0001$, subject $F_{(14,126)} = 2.93$, $p = 0.0007$, interaction $F_{(18,126)} = 4.81$, $p < 0.0001$. *p*-values were determined by *post hoc* Holm–Sidak multiple-comparisons test. ***E***, Relative to WT littermates, full *Adra2a*$^{-/-}$ mice show a loss of guanfacine activity at autoreceptor α_{2A}-ARs, a deficit rescued in the heteroceptor-specific *Adra2a*$^{-/-}$ mice ($F_{(2,12)} = 27.94$, $p < 0.0001$). $n = 5–6$ slices from 3 animals per group. ***F***, Schematic showing timeline of animal habituation, injection, and immunofluorescence. ***G***, Representative images of NeuN (red) and cfos (green) expression after saline and guanfacine injections in WT (***B***), full *Adra2a*$^{-/-}$ (KO, ***C***), and heteroceptor-specific *Adra2a*$^{-/-}$ (KO+TG, ***D***) mice. ***H***, Guanfacine-induced cfos expression in NeuN^{+} cells was higher after guanfacine injection than after saline injection only in WT mice, but not in full or heteroceptor-specific *Adra2a*$^{-/-}$ littermates. Elevated saline-induced cfos expression was observed in full but not heteroceptor-specific *Adra2a*$^{-/-}$ mice relative to WT littermates. $n = 12–26$ animals per group. Two-way ANOVA: treatment effect $F_{(1,105)} = 5.24$, $p = 0.02$, genotype effect $F_{(2,105)} = 0.88$, $p = 0.42$, interaction $F_{(2,105)} = 11.62$, $p < 0.0001$. *p*-values were determined by *post hoc* Holm–Sidak multiple-comparisons test. All data are shown as means ± SEM. *$p < 0.05$, **$p < 0.01$, ***$p < 0.001$, ****$p < 0.0001$, N.S. $p > 0.05$.

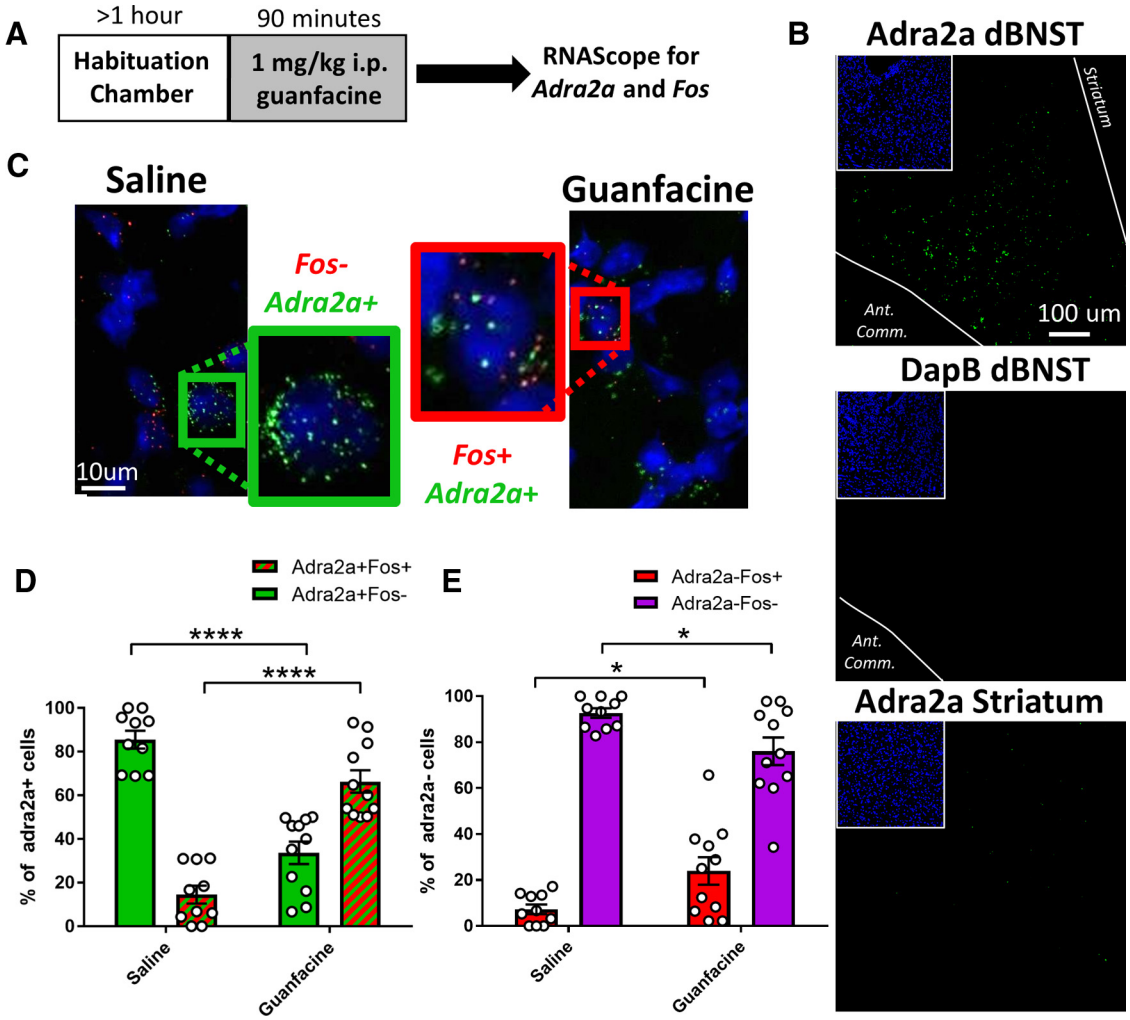

Figure 2. Guanfacine induces cfos expression in dBNST ^{Adra2a} neurons. ***A***, Schematic showing timeline of animal habituation, injection, and RNA scope. ***B***, Anatomical validation of *Adra2a* probe specificity showing significant expression in dBNST (top) alongside lack of negative control bacterial probe *DapB* in dBNST (middle) and lack of *Adra2a* expression in α_{2C}-AR-expressing dorsal striatum. ***C***, Representative images of DAPI $^{+}$ nuclei (blue) as well as the transcripts *Adra2a* (green) and *Fos* (red) after saline and guanfacine injections. Inset, Higher-magnification visualization of a representative *Adra2a* $^{+}$*Fos* $^{-}$ (***B***) and *Adra2a* $^{+}$*Fos* $^{+}$ (***C***) cell after saline and guanfacineinjections, respectively. ***D***, *Adra2a* $^{+}$ cells are largely *Fos* $^{-}$ (85.5 ± 4.1%) after saline injection but upregulate *Fos* after guanfacine injection (66.3 ± 5.1% *Fos* $^{+}$). All data are shown as means ± SEM. *p*-values were determined by unpaired *t* test. **p* < 0.05, *****p* < 0.0001. *n* = 10–11 animals per group.

Guanfacine-induced cfos responses occur in dBNST ^{Adra2a} neurons

Next, we aimed to determine the population of dBNST neurons that express cfos after guanfacine administration. Due to lack of antibody specificity for the α_{2A}-AR, we used *Adra2a* transcript expression as a means of identification (Fig. 2*A*,*B*). The *Adra2a* probe was anatomically validated by observation within the dBNST (Fig. 2*B*, top) alongside a lack of detectable expression of the negative control bacterial probe *DapB* in the dBNST (Fig. 2*B*, middle) and in the α_{2A}-AR-lacking dorsal striatum within the same coronal section (Fig. 2*B*, bottom) (Nicholas et al., 1993). On average, the density of *Adra2a*$^{+}$ cells in the dorsal BNST was 282 ± 45 cells/mm^{2} in saline-injected animals and 269 ± 56 in guanfacine-injected animals, representing 31.8 ± 3.9% and 28.6 ± 5.9% of DAPI $^{+}$ cells, respectively. The difference between either of these values was not statistically significant (unpaired *t* tests, $p = 0.85$ and $p = 0.64$). We monitored *Fos* transcript expression within *Adra2a* $^{+}$ cells 90 min after saline or guanfacine injections (Fig. 2*C*). Treatment with guanfacine significantly increased the percentage of *Adra2a* $^{+}$ cells that were also *Fos* $^{+}$ (14.5 ± 4.1% saline vs 66.3 ± 5.1% guanfacine, unpaired *t* test, $p < 0.0001$; Fig. 2*D*). In addition, treatment with guanfacine led to a small but significant increase in the percentage of *Adra2a* $^{-}$ cells that were *Fos* $^{+}$ (7.3 ± 2.1% saline vs 24.0 ± 6.0% guanfacine, unpaired *t* test, $p = 0.02$; Fig. 2*E*). Therefore, guanfacine injection leads to upregulation of *Fos* within *Adra2a* $^{+}$ and *Adra2a* $^{-}$ cells within the dBNST.

In an effort to better classify *Adra2a* $^{+}$ dBNST cells, we aimed to colocalize *Adra2a* transcript expression with a number of genetic markers known to be expressed in subpopulations of dBNST neurons. *Adra2a* colocalization was modest with the transcripts *Prkcd* (29.8 ± 3.1%), *Penk* (35.5 ± 6.3%), *Calb2* (29.7 ± 8.5%), *Crh* (24.1 ± 8.1%), and *Npy* (9.2 ± 0.3%), suggesting that the *Adra2a* $^{+}$ population is a heterogeneous one.

Guanfacine-induced cfos expression is dBNST autonomous

Upregulation of cfos/*Fos* can be achieved through several mechanisms, some due to direct pharmacological action and others by indirect effects on circuitry. To gain insight into whether guanfacine-induced cfos expression in the dBNST resulted from

interactions with other brain regions in an experience-dependent manner, we combined the use of a *cfos-eGFP* transgenic mouse strain that expresses a GFP-labeled cfos fusion protein (Barth et al., 2004) with thick slice immunohistochemistry (Kupferschmidt et al., 2015) to determine whether guanfacine-induced cfos expression could be mimicked in an *ex vivo* brain slice. Coronal sections (300 μm thick) containing the dBNST were exposed to ACSF, the α_{2A}-AR agonist guanfacine (1 μM) (pEC_{50} = 7.1–7.3) (MacLennan et al., 1997; Jasper et al., 1998), the α_2-AR antagonist atipamezole (1 μM) (pK_i = 8.4–9.5) (Blaxall et al., 1991; Vacher et al., 2010; Vucicevic et al., 2016), or a combination of guanfacine and atipamezole for 1 h at 28°C. Slices were fixed and stained for NeuN to identify neurons and GFP to quantify cfos-eGFP expression (Fig. 3*A*). cfos-eGFP$^+$ cells were readily identified with minimal background activity and quantified as a proportion of neuronal cells (Fig. 3*B*,*C*). A two-way ANOVA showed a significant effect of guanfacine ($F_{(1,44)}$ = 12.39, p = 0.001) and atipamezole ($F_{(1,44)}$ = 12.04, p = 0.001), as well as a significant interaction between the two ($F_{(1,44)}$ = 18.22, p = 0.0001). A Holm–Sidak multiple-comparisons test showed significant upregulation of cfos in guanfacine-incubated slices relative to ACSF-incubated controls (control: 10.9 ± 1.8%, guanfacine: 28.3 ± 3.0%, $p < 0.0001$) and no effect of atipamezole relative to ACSF-incubated controls (atipamezole: 12.7 ± 2.0%, p = 0.92). Incubation of slices in guanfacine and atipamezole did not alter cfos expression relative to ACSF-incubated controls (guanfacine and atipamezole: 11.0 ± 2.1%, p = 0.97) or atipamezole-incubated samples (p = 0.92), but did block guanfacine-induced cfos expression ($p < 0.0001$). Therefore, guanfacine is capable of inducing cfos expression in *ex vivo* dBNST slices and this expression can be blocked by coincubation with the α_2-AR antagonist atipamezole.

Ex vivo incubation in clonidine and UK-14304 induces cfos expression in dBNST neurons

To determine the specificity of guanfacine-induced cfos expression, *ex vivo* dBNST slices were incubated with other α_2-AR agonists. We incubated slices in 10 μM clonidine, a α_2-AR partial agonist, and 10 μM UK-14304, a α_2-AR full agonist, alongside 1 μM guanfacine as a positive control and ACSF as a negative control (Fig. 3*D*,*E*). A one-way ANOVA showed a significant effect of drug incubation on *ex vivo* cfos-eGFP expression ($F_{(3,32)}$ = 4.63, p = 0.009). A Holm–Sidak multiple-comparisons test showed that, relative to ACSF-incubated controls (214 ± 68 cells/mm^2), cfos-eGFP expression was upregulated after exposure to guanfacine (826 ± 174 cells/mm^2; p = 0.02), clonidine (878 ± 161 cells/mm^2; p = 0.02), and UK-14304 (854 ± 167 cells/mm^2; p = 0.02). There were no significant differences between slices incubated in the different α_2-AR agonists (guanfacine vs clonidine, p = 0.99; guanfacine vs UK-14304, p = 0.99, clonidine vs UK-14304, p = 0.99). Therefore, all three of these α_2-AR agonists can induce cfos-eGFP expression *ex vivo* in dBNST sections.

Activation of hM4Di in dBNST neurons by CNO mimics guanfacine-induced cfos induction

To determine whether guanfacine-induced cfos expression is translatable to other G_i-coupled GPCRs, we virally introduced the chemogenetic receptor hM4Di:mCherry or mCherry-encoding control constructs under the control of the CaMKIIα promoter in dBNST neurons and evaluated expression of cfos-eGFP after intraperitoneal injections of guanfacine (1 mg/kg) and CNO (3 mg/kg) alone or in combination (Fig. 4*A*,*B*). In hM4Di-injected mice, a two-way ANOVA showed a significant effect of both CNO ($F_{(1,31)}$ = 5.23, p = 0.03) and guanfacine ($F_{(1,31)}$ = 9.68, p = 0.004), as well as a significant interaction ($F_{(1,31)}$ = 21.18, $p < 0.0001$) on the number of cfos-eGFP$^+$ cells (Fig. 4*C*). A Holm–Sidak multiple-comparisons test determined significant increases relative to saline-injected controls (60 ± 11 cells/mm^2) for guanfacine (213 ± 17 cells/mm^2, $p < 0.0001$), CNO (196 ± 28 cells/mm^2, p = 0.0002), and guanfacine and CNO (167 ± 18 cells/mm^2, p = 0.0028). There were no differences among animals injected with guanfacine and CNO alone or in combination (guanfacine vs CNO, p = 0.56; guanfacine vs guanfacine and CNO, p = 0.29; CNO vs guanfacine and CNO, p = 0.50). A similar distribution was obtained when the number of cfos-eGFP$^+$ cells were quantified as a proportion of hM4Di:mCherry$^+$ cells (Fig. 4*D*). A two-way ANOVA showed a significant effect of guanfacine ($F_{(1,28)}$ = 5.36, p = 0.03) and a significant interaction between guanfacine and CNO ($F_{(1,28)}$ = 5.36, p = 0.03), but no effect of CNO alone ($F_{(1,28)}$ = 1.244, p = 0.27). A Holm–Sidak multiple-comparisons test showed significant upregulation of cfos-eGFP relative to saline injected controls (7.5 ± 1.5% of hM4Di:mCherry$^+$ cells) in animals injected with guanfacine (26.2 ± 5.7%; p = 0.003), CNO (21.6 ± 5.8%; p = 0.01), and guanfacine and CNO (21.3 ± 2.4%; p = 0.02). There were no statistically significant differences among animals injected with guanfacine, CNO, or guanfacine and CNO (guanfacine vs CNO, p = 0.72; guanfacine vs guanfacine and CNO, p = 0.38; CNO vs guanfacine and CNO, p = 0.66). Therefore, CNO activation of hM4Di induces a cfos response in BNST neurons that is equivalently sized and blocks further guanfacine-induced cfos expression.

In mCherry-injected controls (Fig. 4*B*, bottom), a two-way ANOVA showed a significant effect of guanfacine ($F_{(1,8)}$ = 116.3, $p < 0.0001$) and CNO ($F_{(1,8)}$ = 6.57, p = 0.04), but no significant interaction ($F_{(1,8)}$ = 0.008, p = 0.93) (Fig. 4*E*). A Holm–Sidak multiple-comparisons test showed significant increases in cfos-eGFP numbers relative to saline-injected controls (64 ± 12 cells/mm^2) for animals injected with guanfacine (239 ± 22 cells/mm^2, p = 0.0003) and guanfacine and CNO (198 ± 18 cells, p = 0.001), but a trend toward decreased cfos expression in CNO-injected animals (21 ± 11 cells, p = 0.19) rather than the increase seen in hM4Di-injected animals. Significant upregulation was also observed relative to CNO-injected animals in guanfacine- and dual guanfacine- and CNO-injected animals (CNO vs guanfacine, $p < 0.0001$; CNO vs guanfacine and CNO, p = 0.0003). There was no difference between guanfacine-injected animals and those injected with both guanfacine and CNO (p = 0.19). Here, we show that CNO does not induce cfos expression without the presence of hM4Di and does not compete with guanfacine-induced cfos expression.

Guanfacine-activated Adra2a$^+$ dBNST neurons express functional HCN subunits

To allow for the study of putative guanfacine-activated neurons more precisely, *cfos-eGFP* mice were injected intraperitoneally with guanfacine (1 mg/kg) 90 min before brain slice preparation and electrophysiological recording (Fig. 5*A*). This strategy allowed for identification of cfos-eGFP-expressing cells that were examined by whole-cell electrophysiology and confirmed by *post hoc* immunohistochemistry (Fig. 5*B*). Current-clamp profiles, defined here as membrane potential responses to positive and negative current injections, were obtained and showed that 8/11 cells had a hyperpolarization sag on negative current injection (average amplitude = 1.9 ± 0.5 mV; Fig. 5*C*). This characteristic response to negative current injection of an initial hyperpolariza-

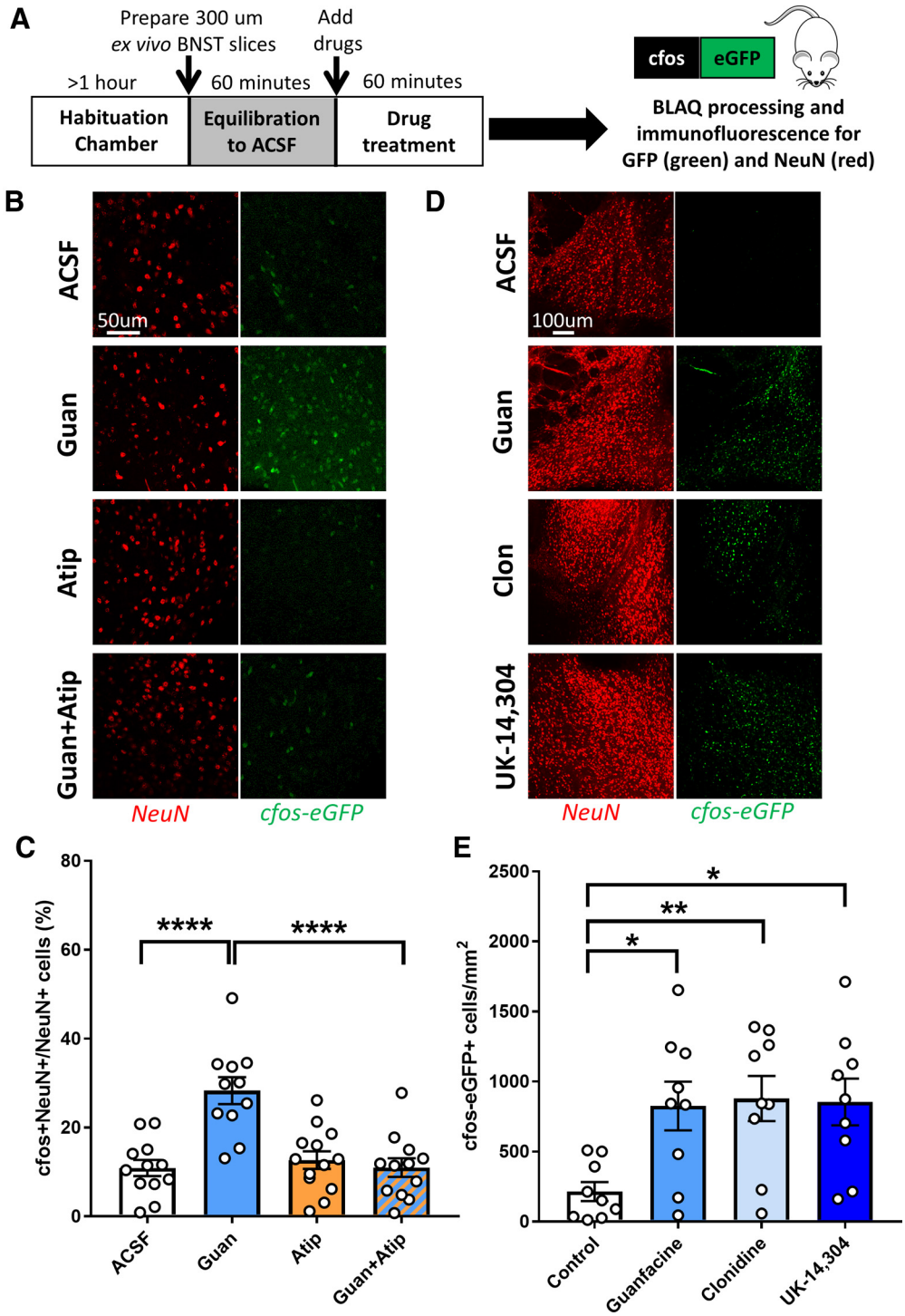

Figure 3. Incubation of *ex vivo* dBNST slices with guanfacine is sufficient to induce cfos expression and can be blocked by atipamezole. ***A***, Schematic showing timeline of animal habituation, slice preparation, drug application, and immunostaining. ***B***, Representative images of NeuN (red) and *cfos-eGFP* expression (green) after incubation in ACSF, guanfacine (1 μM), atipamezole (1 μM), or simultaneous application of guanfacine and atipamezole (1 μM each). Two-way ANOVA: guanfacine effect $F_{(1,44)} = 12.39$, $p = 0.001$, atipamezole effect $F_{(1,44)} = 12.04$, $p = 0.001$, interaction $F_{(1,44)} = 18.22$, $p = 0.0001$. ***C***, Guanfacine incubation induces cfos-eGFP expression compared with ACSF-incubated controls. Atipamezole incubation does not alter dBNST cfos-eGFP expression but does block guanfacine-induced cfos induction to almost control levels. ***D***, Representative images of NeuN (red) and cfos-eGFP expression (green) after incubation in ACSF, guanfacine (1 μM), clonidine (10 μM), or UK-14304 (10 μM). ***E***, Guanfacine, clonidine, and UK-14304 significantly upregulate cfos-eGFP expression compared with ACSF-incubated control slices. All data are shown as means ± SEM. One-way ANOVA: drug effect $F_{(3,32)} = 4.63$, $p = 0.009$. *p*-values were obtained from *post hoc* Holm–Sidak multiple-comparisons test. $^*p < 0.05$, $^{**}p < 0.01$, $^{****}p < 0.0001$. $n = 9$–13 animals represented across all groups.

tion followed by a slower depolarization is generally suggestive of underlying HCN channel activity (Wahl-Schott and Biel, 2009). A 1 h incubation of the slices with the HCN channel inhibitor ZD7288 (10 μM) abolished this sag in 10/11 cells recorded (0.09 ± 0.09 mV; Fig. 5*D*). The difference between untreated and ZD7288-treated slices was significant (unpaired *t* test, $p = 0.001$; Fig. 5*E*). Kinetic analyses were performed on the hyperpolarization sag aiming to uncover which of the four mammalian HCN

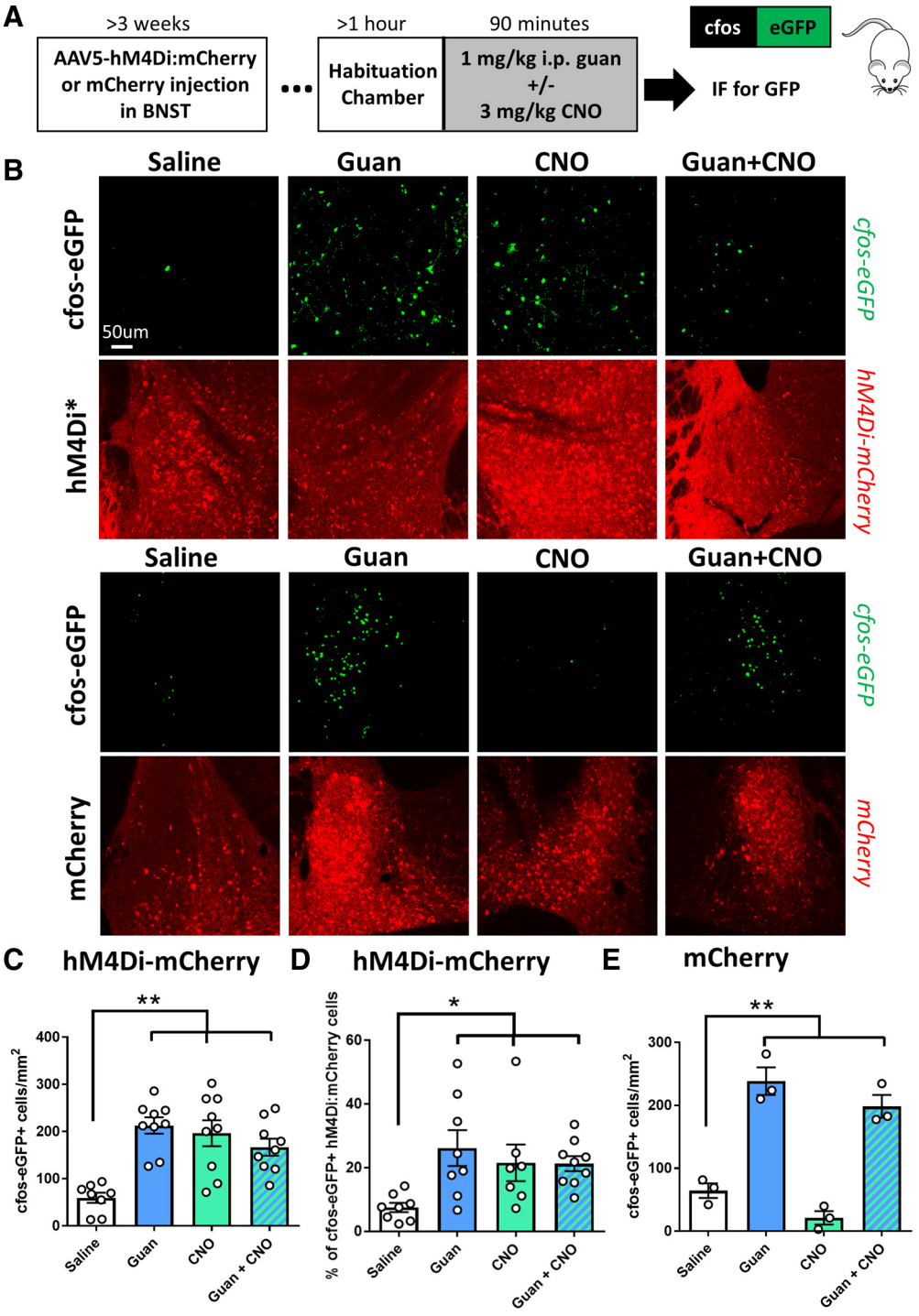

Figure 4. Activation of hM4Di in dBNST neurons by CNO mimics guanfacine-induced cfos expression *in vivo*. ***A***, Schematic showing timeline of animal habituation, AAV vector injection, drug injection, and immunofluorescence. ***B***, Representative images of cfos-eGFP (green) and hM4Di:mCherry (red, top) or mCherry (red, bottom) expression in the dBNST; animals were injected with saline, guanfacine (1 mg/kg), CNO (3 mg/kg), or guanfacine and CNO. ***C***, Injections of guanfacine and CNO alone or in combination lead to increased cfos-eGFP expression relative to saline-injected controls in mice expressing hM4Di in the dBNST. There were no differences in cfos-eGFP levels among hM4Di-expressing animals injected with guanfacine or CNO alone or in combination. Two-way ANOVA: CNO effect $F_{(1,31)} = 5.229$, $p = 0.029$, guanfacine effect $F_{(1,31)'} = 9.68$, $p = 0.004$, interaction $F_{(1,31)} = 21.18$, $p < 0.0001$. ***D***, Injections of guanfacine (1 mg/kg) and CNO (3 mg/kg) alone or in combination lead to increased dBNST cfos-eGFP expression in hM4Di:mCherry $^{+}$ cells relative to saline-injected controls in hM4Di-expressing mice. There were no differences in cfos-eGFP levels among hM4Di-expressing animals injected with guanfacine or CNO alone or in combination. Two-way ANOVA: CNO effect $F_{(1,28)} = 1.244$, $p = 0.27$, guanfacine effect $F_{(1,28)'} = 5.36$, $p = 0.03$, interaction $F_{(1,28)} = 5.36$, $p = 0.03$. ***E***, Injections of guanfacine (1 mg/kg) with or without CNO (3 mg/kg) led to increased cfos-eGFP expression relative to saline- and CNO-injected mCherry-expressing controls. Addition of CNO did not significantly affect either saline- or guanfacine-induced cfos expression levels. Two-way ANOVA: CNO effect: $F_{(1,8)} = 6.57$, $p = 0.04$, guanfacine effect $F_{(1,8)} = 116.3$, $p < 0.0001$, interaction $F_{(1,8)} = 0.01$, $p = 0.93$. All *p*-values were determined by *post hoc* Holm–Sidak multiple-comparisons test. $n = 3$–9 mice per group. $^{*}p < 0.05$, $^{**}p < 0.01$. All data are shown as means ± SEM.

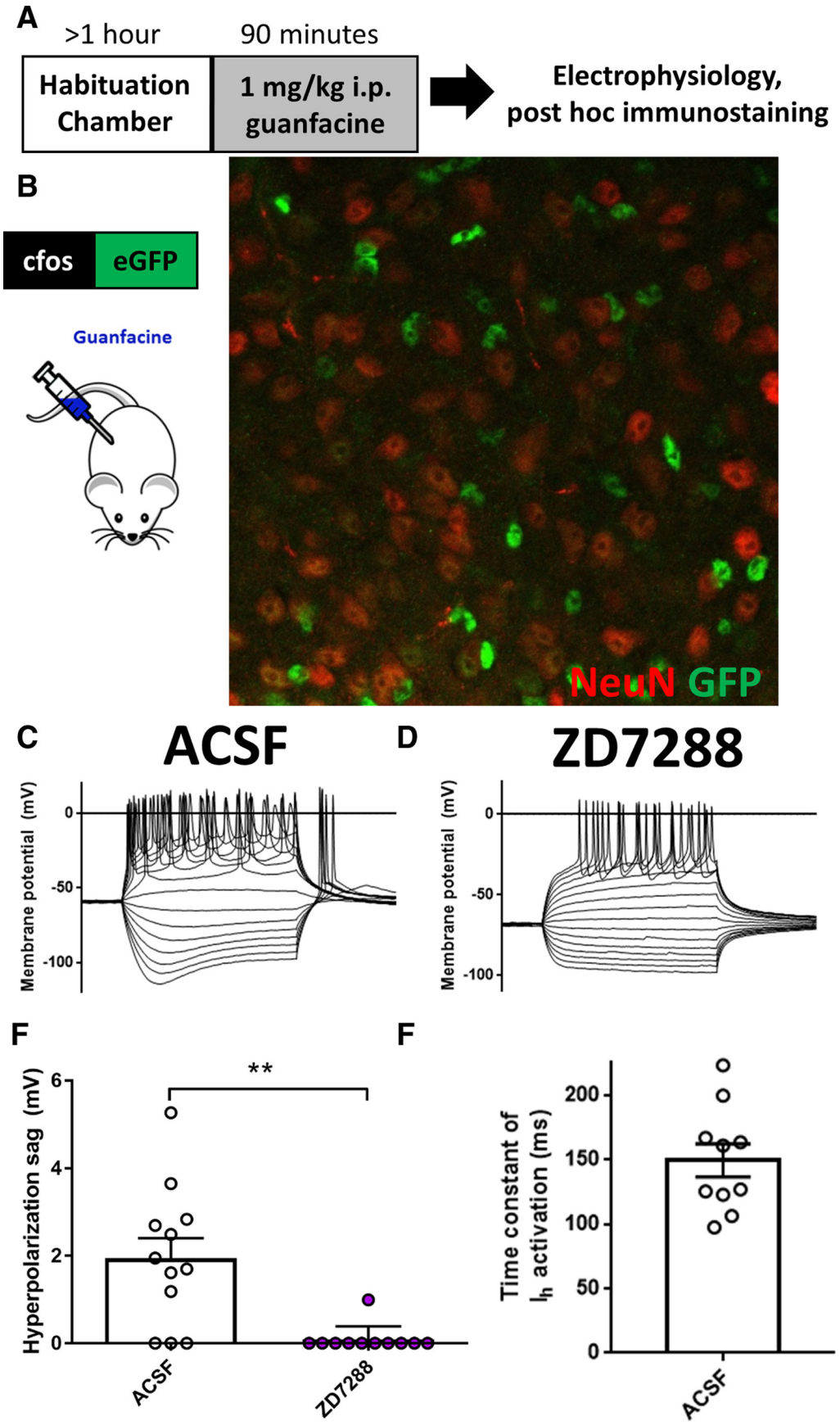

Figure 5. dBNST neurons that express cfos after systemic guanfacine administration show a high prevalence of HCN activity. ***A***, Schematic showing timeline for *cfos-eGFP* animal habituation, guanfacine injection, and slice preparation for electrophysiology and immunostaining. ***B***, Representative image showing the expression of *cfos-eGFP* (green) and NeuN $^+$ neurons (red) in the dBNST in a *post hoc* fixed 300-μm-thick slice that was stained after electrophysiological recording. ***C–E***, Current-clamp profiles of cfos-eGFP $^+$ dBNST neurons. (*Figure legend continues.*)

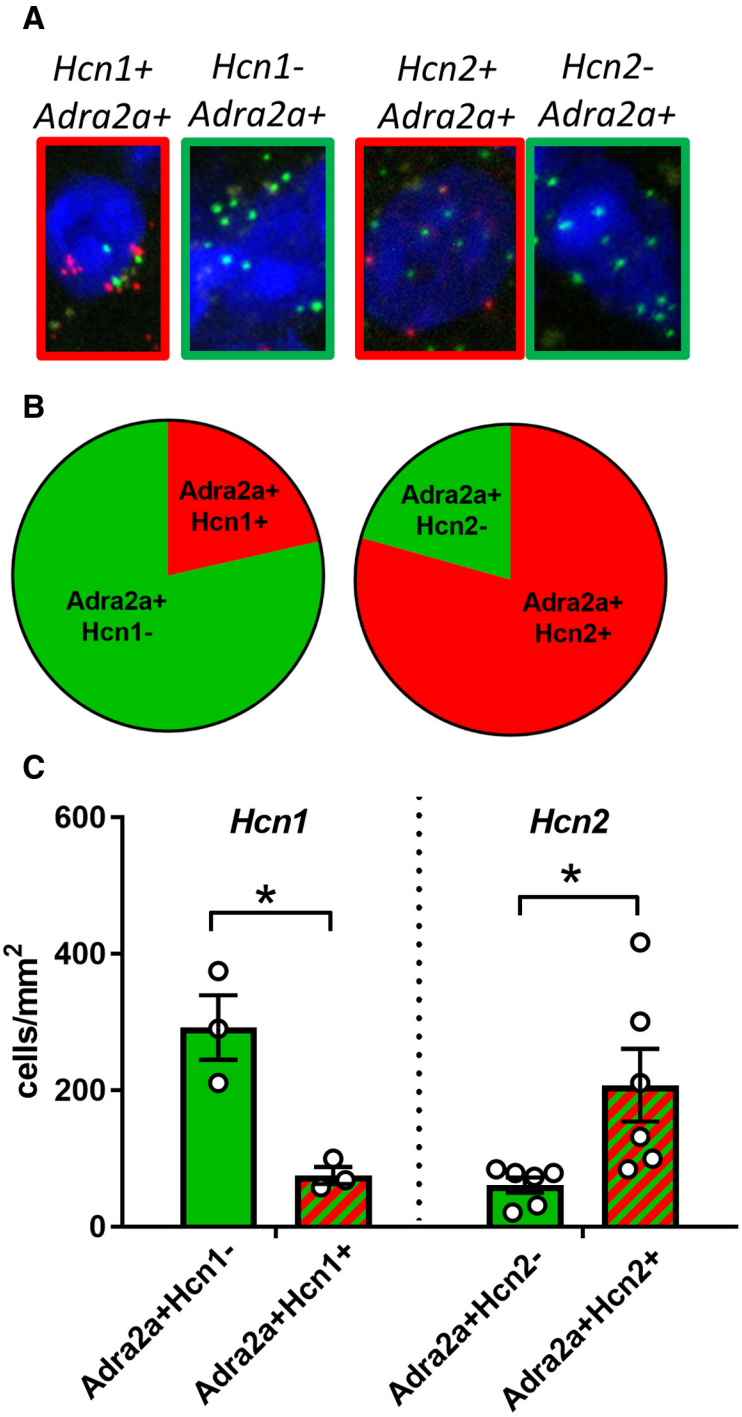

Figure 6. A majority of Adra2a$^+$ dBNST neurons coexpress Hcn2, whereas a minority coexpress Hcn1. ***A***, Representative images of DAPI$^+$ nuclei (blue) in dBNST that express *Adra2a* transcripts (green) with or without either *Hcn1* transcripts (red, left) or *Hcn2* transcripts (red, right). ***B***, As a proportion of *Adra2a*$^+$ cells, 21.5 ± 5.4% coexpress *Adra2a* and *Hcn1* transcripts while 71.4 ± 7.3% coexpress *Adra2a* and *Hcn2* transcripts. ***C***, The number of *Adra2a*$^+$*Hcn1*$^-$ cells is greater than the number of *Adra2a*$^+$*Hcn1*$^+$ cells, whereas the number of *Adra2a*$^+$*Hcn2*$^+$ cells is greater than the number of *Adra2a*$^+$*Hcn2*$^-$ cells. *p*-values were determined by unpaired *t* test. *$p < 0.05$. All data are shown as means ± SEM.

←

(*Figure legend continued.*) The characteristic hyperpolarization sag indicating HCN channel activity was seen in control recordings (ACSF incubation) (***C***), but not after incubation in 10 μM ZD7288 (***D***). *p*-values were calculated from an unpaired *t* test. **$p < 0.01$. $n = 11$–12 cells from 4–5 mice. ***F***, Kinetic analyses of the hyperpolarization sag show an average time constant of I_h activation of 149.2 ± 12.9 ms, suggesting HCN1 or HCN2 expression. All data are shown as means ± SEM.

channel subunits (HCN1–HCN4) may constitute the pacemaker current in dBNST neurons. The average τ of activation calculated from the point of maximal hyperpolarization to the steady-state potential was 149.2 ± 12.9 ms (range 97.4–223 ms; Fig. 5*F*), suggesting involvement of HCN1 or HCN2 subunits that display similar values either in homomeric or heteromeric channels (Ulens and Tytgat, 2001).

A FISH approach was used to confirm HCN transcript expression in *Adra2a*$^+$ dBNST neurons (Fig. 6*A*). On average, the density of transcript-positive cells within the dBNST was 301 ± 37 cells/mm^2 for *Adra2a*$^+$ cells (representing 34.5 ± 3.3% of DAPI$^+$ cells), 127 ± 24 for *Hcn1*$^+$ cells (15.3 ± 4.7% of DAPI$^+$ cells), and 550 ± 85 for *Hcn2*$^+$ cells (62.1 ± 6.4% of DAPI$^+$ cells). Although a majority of *Adra2a*$^+$ cells were negative for *Hcn1* transcripts (78.6 ± 5.4%), a large fraction was positive for *Hcn2* transcripts (71.4 ± 7.3%; Fig. 6*B*). Unpaired *t* tests on the number of cells observed (Fig. 6*C*) confirmed that *Adra2a*$^+$ cells are more likely to be *Hcn1*-negative than to express *Hcn1* transcripts (*Adra2a*$^+$*Hcn1*$^+$: 76 ± 13 cells/mm^2; *Adra2a*$^+$*Hcn1*$^-$: 292 ± 62 cells/mm^2; $p = 0.04$) and more likely to be *Hcn2*$^+$ than to not express *Hcn2* transcripts (*Adra2a*$^+$*Hcn2*$^+$: 208 ± 53 cells/mm^2; *Adra2a*$^+$*Hcn2*$^-$: 62 ± 11 cells/mm^2; $p = 0.04$). In addition to expressing cfos transcripts after guanfacine injection, a majority of *Adra2a*$^+$ cells also coexpress *Hcn2* transcripts.

HCN channel inhibition is sufficient for excitatory actions on glutamatergic transmission in the dBNST

Colocalization of *Adra2a* and *Hcn2* transcripts suggests that receptor-dependent signaling might have an impact on HCN channel activity. In prefrontal cortex, postsynaptic α_{2A}-ARs enhance glutamatergic transmission by inhibition of HCN channels through a process whereby decreased postsynaptic cAMP decreases the HCN channel open probability and diminishes HCN-dependent filtering of synaptic currents passing through the dendritic neck (Wang et al., 2007). We tested the effects of the HCN channel inhibitor ZD7288 on optically evoked excitatory transmission in a Thy1-COP4 transgenic mouse line (line 9). This mouse line expresses a transgene encoding channelrhodopsin-2 (ChR2) under the control of the thymus cell antigen 1 (Thy1) promoter randomly inserted into the genome, which as a result leads to expression within subsets of projection neurons across the brain, including neurons from the cortex, hippocampus, thalamus, midbrain, brainstem, cerebellar mossy

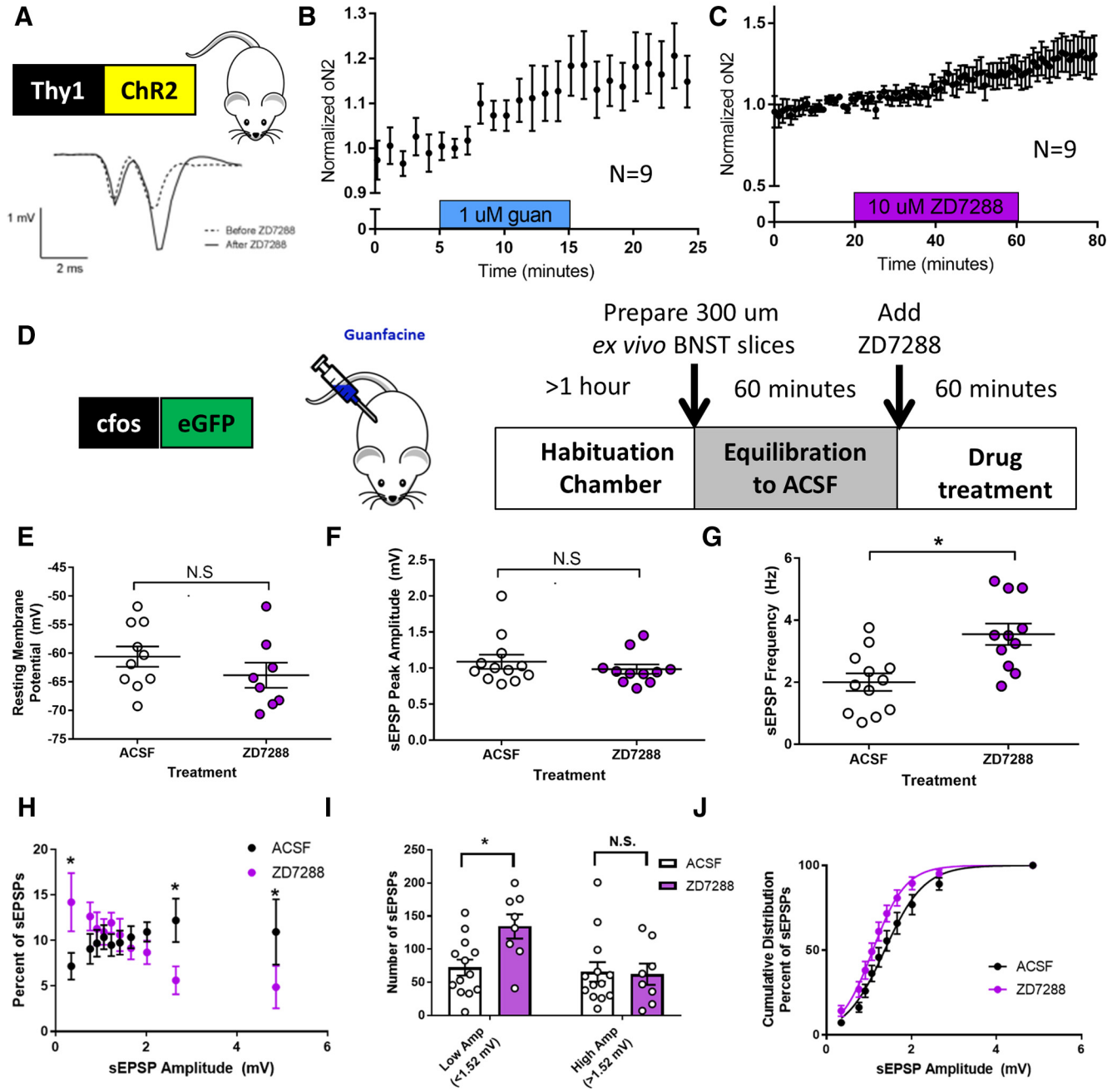

Figure 7. HCN channel inhibition by ZD7288 is sufficient for excitatory actions on glutamatergic transmission within the dBNST. ***A***, Representative trace of an optically evoked field potential in the dBNST of Thy1-COP4 mice showing an oN1 and oN2 component analogous to electrically evoked field potentials in the region. ***B***, Guanfacine application (1 μM for 10 min) enhanced oN2 amplitude by 15.9 $\pm$ 6.0% in the dBNST of Thy1-COP4 mice. $n = 9$ slices from 4 mice. ***C***, ZD7288 application (10 μM for 40 min) also enhanced oN2 amplitude by 18.7 $\pm$ 7.6% in the dBNST of Thy1-COP4 mice. $n = 9$ slices from 5 mice. ***D***, Schematic showing the timeline of *cfos-eGFP* animal habituation, slice preparation, ZD7288 (10 μM) incubation, and electrophysiology recording. ***E–G***, ZD7288 incubation did not affect resting membrane potential and had no effect on sEPSP amplitude in cfos-eGFP $^{+}$ dBNST neurons, but did increase sEPSP frequency. ***H–J***, ZD7288 preincubation increased the proportion of low-amplitude sEPSPs and decreased the proportion of high-amplitude sEPSPs among all sEPSPs, increased only the number of low-amplitude sEPSPs (<1.52 mV), and caused a leftward shift in the cumulative frequency distribution of sEPSP amplitudes relative to ACSF preincubated controls. Two-way ANOVA on sEPSP amplitude proportion: drug effect ($F_{(1,190)} = 2 \times 10^{-14}$, $p > 0.9999$), amplitude effect ($F_{(9,190)} = 0.48$, $p = 0.89$), interaction ($F_{(9,190)} = 2.35$, $p = 0.02$. Two-way ANOVA on sEPSP amplitude number: drug effect ($F_{(1,19)} = 3.44$, $p = 0.08$, amplitude effect ($F_{(1,19)} = 6.89$, $p = 0.02$), interaction ($F_{(1,19)} = 4.75$, $p = 0.04$). Nonlinear regression line of best fit comparison: ($F_{(2,206)} = 16.27$, $p < 0.0001$. *p*-values were determined by unpaired *t* tests (***E–G***), Fisher's LSD analysis (***H***), or Holm–Sidak (***I***) multiple-comparisons test. N.S. $p > 0.05$, *$p < 0.05$. All data are shown as means $\pm$ SEM.

fibers, and retinal ganglion cells (Arenkiel et al., 2007). Importantly, this mouse line has been shown to minimally express ChR2 in dBNST neurons and shows little to no colocalization of ChR2 with calcitonin gene-related peptide (CGRP), a high-fidelity marker of the guanfacine-inhibited parabrachial nucleus afferents within the dBNST (Flavin et al., 2014). Use of this mouse line thus allows for enrichment of light-induced presynaptic release of glutamate from non-parabrachial nucleus afferents within the dBNST. The pattern of activity elicited by *ex vivo* optical stimulation within the dBNST in this mouse strain was previously shown to unmask excitatory actions of guanfacine, presumably due to the lack of presynaptic inhibition of glutamate release by α_{2A}-AR activity at parabrachial nucleus terminals (Flavin et al., 2014). In this experiment, optically evoked field poten-

tials were observed as two negative deflections defined here as oN1 and oN2, analogous to the fiber volley potential N1 and synaptic potential N2 observed in electrically evoked field potential recordings in the dBNST (Fig. 7*A*).We first replicated previous findings that bath application of guanfacine (1 μM) for 10 min significantly increases the amplitude of oN2 by 15.9 ± 6.0% (range: −17.3 to +67.7%; paired *t* test, $p = 0.03$; Fig. 7*B*). Then, in a separate cohort of animals, we bath applied ZD7288 (10 μM) for 40 min, which increased the oN2 amplitude by 18.7 ± 7.6% (range: −14.1 to +53.4%; paired *t* test, $p = 0.04$; Fig. 7*C*).

To gain insight into potential cell-type-specific effects of ZD7288, we recorded from cfos-eGFP$^+$ cells 90 min after guanfacine injection (Fig. 7*D*). To maximize potential activation of endogenous HCN channels by avoiding voltage-clamp-mediated inhibition and to minimize loss of HCN current observation and modulation due to long-term cell dialysis, sEPSPs were recorded in cfos-eGFP$^+$ cells after a 1 h incubation in ZD7288 or vehicle (10 μM; Fig. 7*D*). ZD7288 incubation did not significantly affect resting membrane potential (control: −60.6 ± 1.8 mV; ZD7288: −63.9 ± 2.2 mV; unpaired *t* test, $p = 0.26$; Fig. 7*E*). The treatment had no effect on average sEPSP amplitude (control: 1.1 ± 0.1 mV; ZD7288: 1.0 ± 0.1 mV; unpaired *t* test, $p = 0.40$; Fig. 7*F*), but did significantly increase sEPSP frequency (control: 2.0 ± 0.3 Hz; ZD7288: 3.6 ± 0.4 Hz; unpaired *t* test, $p = 0.002$; Fig. 7*G*). An increase in sEPSP frequency is classically interpreted as resulting from modulation of presynaptic glutamate release. However, an increase in sEPSP frequency could also result from release of dendritic filtering on synapses distant from the location of somatic recording with resulting low-amplitude spontaneous events (Larkum et al., 1998; Williams and Mitchell, 2008; Gantz et al., 2013). To differentiate between these possibilities, we evaluated the distribution of events across amplitudes in ACSF- and ZD7288-preincubated slices (Figs. 7*H–J*). When comparing the frequency distribution of sEPSP amplitudes with or without ZD7288 preincubation, a two-way ANOVA showed a significant interaction between drug treatment and amplitude ($F_{(9,190)} = 2.35$, $p = 0.02$), but no effect of drug ($F_{(1,190)} = 2 \times 10^{-14}$, $p > 0.9999$) or amplitude ($F_{(9,190)} = 0.48$, $p = 0.89$) alone. Fisher's LSD analysis showed significant differences between the treatments at the lowest-amplitude bin (<0.7 mV, ACSF = 7.2 ± 1.5%, ZD7288 = 14.2 ± 3.2%, $p = 0.01$) and the two highest-amplitude bins (2.2 to 3.1 mV, ACSF = 12.2 ± 2.4%, ZD7288 = 5.6 ± 1.5%, $p = 0.02$; >3.1 mV, ACSF = 10.9 ± 3.6%, ZD7288 = 4.9 ± 2.3%, $p = 0.03$), with ZD7288 preincubation increasing the frequency of low-amplitude events and decreasing the frequency of high-amplitude events as a proportion of all events. To determine whether this change in frequency distribution is due to increased numbers of low-amplitude events or decreased high-amplitude events, we compared the number of events with amplitudes greater than or less than 1.52 mV, the point of intersection for the frequency distributions across drug treatments. Here, by repeated-measures two-way ANOVA, we observed a significant effect of amplitude ($F_{(1,19)} = 6.89$, $p = 0.02$) and a significant interaction between amplitude and drug treatment ($F_{(1,19)} = 4.75$, $p = 0.04$), but no effect of treatment alone ($F_{(1,19)} = 3.44$, $p = 0.08$). A Holm–Sidak multiple-comparisons test showed that ZD7288 preincubation increased the number of low-amplitude events (ACSF = 72.3 ± 12.0 events, ZD7288 = 134.4 ± 18.2 events, $p = 0.01$), with no difference in high-amplitude events (ACSF = 65.6 ± 14.8 events, ZD7288 = 62.1 ± 16.1 events, $p = 0.98$). Finally, in comparing the cumulative frequency distribution between the treatments and fitting a nonlinear line of best fit to the data (Fig. 7*J*), we observed a left shift after ZD7288 preincubation and a difference in the line of best fit when constraining the maximum (100%) and minimum (0%) curve parameters and varying the Hill coefficient (ACSF = 0.94 ± 0.09, ZD7288 = 1.12 ± 0.10) and IC_{50} (ACSF = 1.37 ± 0.04 mV, ZD7288 = 1.124 ± 0.03 mV). Using different parameters for each of the datasets resulted in a better fit of the data ($F_{(2,206)} = 16.27$, $p < 0.0001$) than using the same parameters for both, confirming that the shape and the amplitude distribution are statistically different. In sum, ZD7288 enhanced spontaneous glutamatergic transmission in cfos-eGFP$^+$ cells after guanfacine injection likely via decreased dendritic filtering of low-amplitude sEPSPs.

shRNA knock-down of HCN1 and HCN2 occludes guanfacine-induced cfos expression

Having demonstrated that HCN channel inhibition causes excitatory actions within the dBNST, we next addressed the question of whether HCN channels are a downstream target of guanfacine actions. To do this, we used AAVs encoding shRNAs directed against both the HCN1 and HCN2 channel subunits (AAV9-shHCN1/2; Fig. 8*A*). Current-clamp responses to positive and negative current injections were obtained from injected animals and sham controls (Fig. 8*B*, *C*). Hyperpolarization sag amplitude was determined from these responses as the difference in membrane potential between the initial maximal negative potential and steady-state potential upon negative current injection. After dual subunit knock-down, the amplitude of the hyperpolarization sag was decreased by 43.8% (sham: 3.0 ± 0.5 mV; shHCN1/2: 1.3 ± 0.4 mV; unpaired *t* test, $p = 0.008$; Fig. 8*D*), validating a functional loss of HCN channel activity. Dual subunit knock-down did not affect resting membrane potential (sham: −80.3 ± 1.6 mV; shHCN1/2: −82.8 ± 2.3 mV; unpaired *t* test, $p = 0.40$), sEPSP frequency (sham: 1.8 ± 0.2 Hz; shHCN1/2: 1.8 ± 0.2 Hz; unpaired *t* test, $p = 0.92$), or sEPSP amplitude (sham: 1.4 ± 0.1 mV; shHCN1/2: 1.7 ± 0.2 mV; unpaired *t* test, $p = 0.35$) in AAV9-shHCN1/2$^+$ BNST neurons, suggesting either that identification of guanfacine-activated neurons is necessary for observation of excitatory effects or that viral knock-down does not mimic acute pharmacological inhibition of HCN channel activity in this regard.

We used the same strategy to test for an interaction between HCN channel activity and guanfacine-induced cfos responses alongside controls injected with a recombinant control virus expressing only GFP (AAV9-GFP; Fig. 8*E*). A two-way ANOVA revealed a significant effect of shRNA injection on cfos$^+$ cells ($F_{(1,16)} = 7.86$, $p = 0.01$), no effect of guanfacine exposure ($F_{(1,16)} = 2.40$, $p = 0.14$), and a trend toward a significant interaction ($F_{(1,16)} = 3.14$, $p = 0.10$) (Fig. 8*F*). A Holm–Sidak multiple-comparisons test showed upregulation of cfos relative to saline-injected AAV9-GFP controls (71 ± 9 cfos$^+$ cells/mm^2) in guanfacine-injected AAV9-GFP controls (102 ± 6 cfos$^+$ cells/mm^2, $p = 0.03$), saline-injected AAV9-shHCN1/2 animals (113 ± 9 cfos$^+$ cells/mm^2, $p = 0.02$), and guanfacine-injected AAV9-shHCN1/2 animals (110 ± 11 cfos$^+$ cells/mm^2, $p = 0.02$). No differences were observed between AAV9-shHCN1/2 animals injected with saline and guanfacine ($p = 0.88$). To begin to assess the behavioral relevance of this difference, the EPM was used to determine anxiety-like behavior in a separate cohort of mice. No baseline differences were observed between AAV9-GFP and AAV9-shHCN1/2 animals in open arm time (GFP: 164.7 ± 14.2 s; shHCN1/2: 163.6 ± 20.2 s; unpaired *t* test, $p = 0.96$), closed arm time (GFP: 91.7 ± 11.1 s; shHCN1/2: 100.1 ± 17.8 s; unpaired *t* test, $p = 0.69$), center zone time (GFP: 105.3 ± 13.2 s; shHCN1/2: 87.4 ± 12.8 s; unpaired *t* test, $p = 0.34$), or total

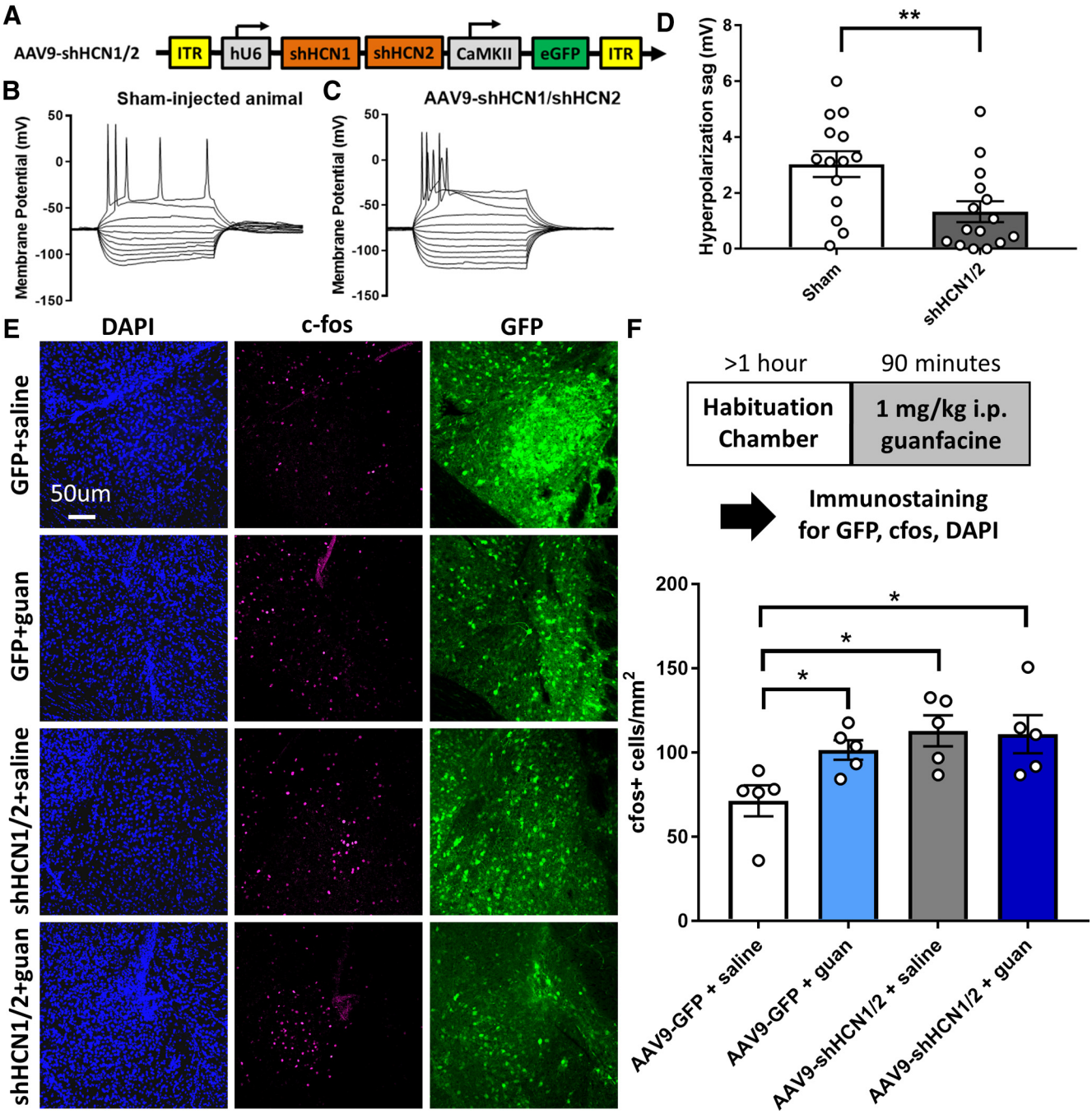

Figure 8. Delivery of shRNAs directed against HCN channel subunits to the dBNST occludes guanfacine-induced cfos expression. ***A***, Schematic of AAV9-shHCN1/2 virus; inverted terminal repeat (ITR), human U6 (hU6) promoter driving expression of *Hcn1* and *Hcn2*-specific shRNAs, *CaMKII* promoter used for neural expression of *eGFP*. ***B***, ***C***, Current-clamp profiles of sham-injected (***B***) and AAV9-shHCN1/2 animals (***C***) show the presence and absence of a hyperpolarization sag, respectively. ***D***, Injection of shHCN1/2-encoding virions reduces the average amplitude of hyperpolarization sag in dBNST neurons. ***E***, Representative images of DAPI $^{+}$ (blue), cfos (magenta), and virally expressed eGFP (green) in dBNST after saline or guanfacine treatment. ***F***, Guanfacine increased cfos expression in AAV9-eGFP control mice but not in mice that were injected with AAV9-shHCN1/2. Expression of cfos in AAV9-shHCN1/2 animals was similar to values were obtained in controls injected with guanfacine, a result reminiscent of cfos expression in *Adra2a* $^{-/-}$ transgenic mice (KO; see Fig. 1). Two-way ANOVA: shRNA effect: ($F_{(1,16)} = 7.86, p = 0.01$), guanfacine effect ($F_{(1,16)} = 2.40, p = 0.14$), interaction ($F_{(1,16)} = 3.14, p = 0.10$). *p*-values were determined by unpaired *t* test (***D***) or *post hoc* Holm–Sidak multiple-comparisons test. $^{*}p < 0.05$, $^{**}p < 0.01$. All data are shown as means ± SEM.

distance traveled (GFP: 7.9 ± 0.6 m; shHCN1/2: 9.3 ± 0.6 m; unpaired *t* test, $p = 0.13$).

Activation of hM4Di in dBNST neurons elicits anxiogenic behavior and activity increases in the EPM

Finally, we aimed to determine the behavioral and physiological relevance of this noncanonical aspect of α_{2A}-AR signaling using CNO activation of the chemogenetic G_i-coupled DREADD receptor hM4Di expressed in dBNST neurons. We recorded dBNST-based Ca^{2+} transients during the EPM from implanted animals tethered to the fiber photometry system by a flexible patch cord. Animals stereotaxically injected with AAV5-GCaMP6f and AAV5-hM4Di or AAV5-mCherry were given an intraperitoneal injection of either saline or CNO (3 mg/kg) 120 min before behavioral testing. Compared with saline-injected AAV5-hM4Di controls, CNO-injected animals showed increased

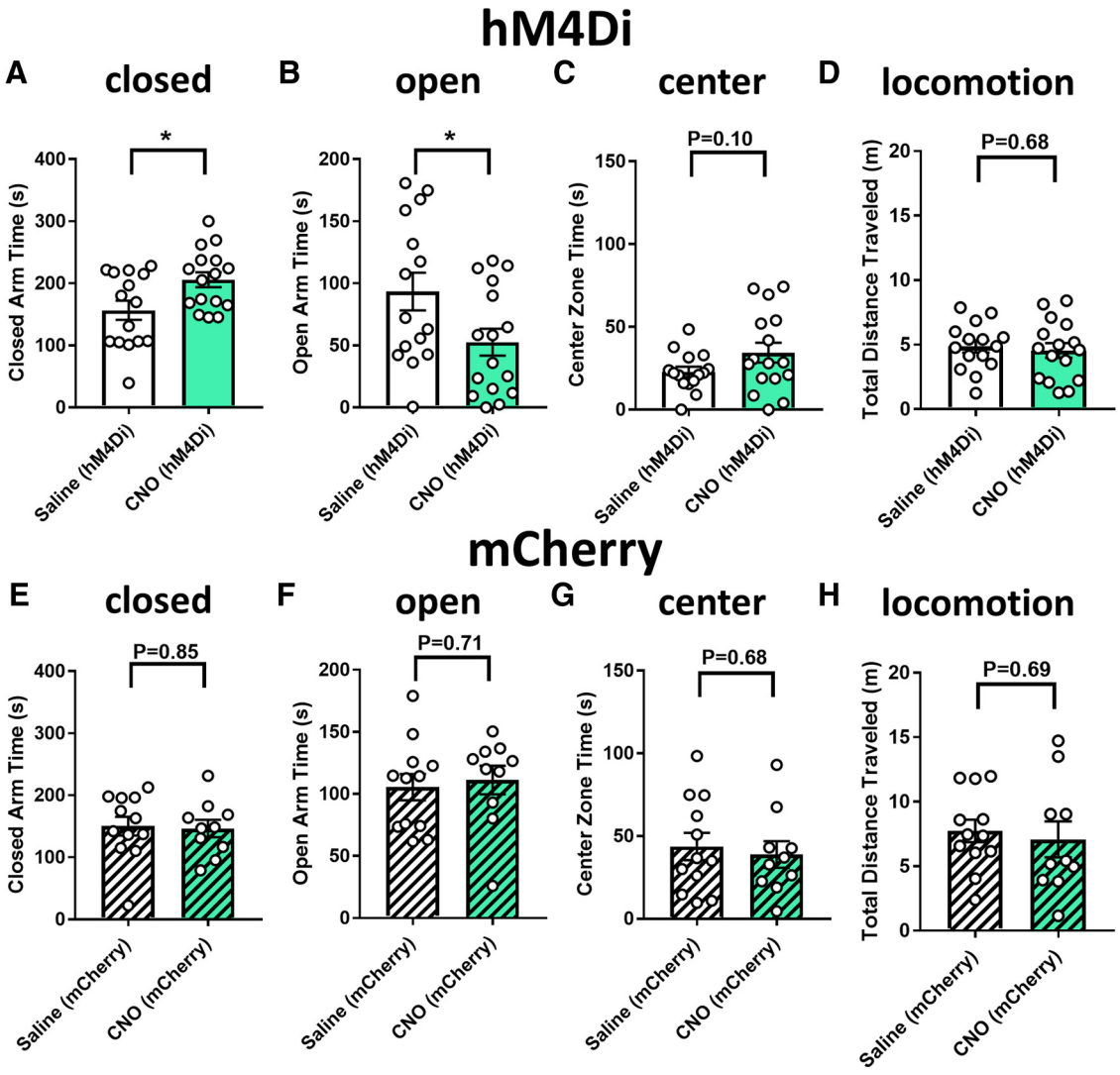

Figure 9. Activation of hM4Di receptors expressed in dBNST neurons elicits anxiety-like behavior in the EPM. ***A–D***, Behavioral data from the EPM showing increased anxiety-like behavior in CNO-injected mice expressing the hM4Di receptor compared with saline-injected control animals. CNO led animals to spend more time in the closed arm (***A***) and, subsequently, less time in the open arm (***B***), with no change in time spent in the center zone (***C***) or total distance traveled (***D***). (***E–H***) No effect was observed after CNO injection in AAV5-mCherry animals during the EPM: no change in time spent in the closed arm (***E***), open arm (***F***), center zone (***G***), and total distance traveled (***H***). *p*-values were calculated by unpaired *t* test. $*p < 0.05$. $n = 10–16$ animals per group. All data are shown as means ± SEM.

anxiety-like behavior as manifested in increased closed arm time (saline: 156.6 ± 15.5 s; CNO: 205.8 ± 12.0 s; unpaired *t* test, $p = 0.02$; Fig. 9*A*) and decreased open arm time (saline: 93.4 ± 15.1 s; CNO: 52.6 ± 10.8 s; unpaired *t* test, $p = 0.03$; Fig. 9*B*). There were no effects on the time spent in the center zone (saline: 22.9 ± 3.0 s; CNO: 34.5 ± 6.0 s; unpaired *t* test, $p = 0.10$; Fig. 9*C*) or locomotion (total distance traveled; saline: 4.9 ± 0.5 m; CNO: 4.6 ± 0.6 m; unpaired *t* test, $p = 0.6790$; Fig. 9*D*). In AAV5-mCherry controls, there were no differences between saline- and CNO-injected animals in the time spent in the closed arm (saline: 150.4 ± 15.3 s; CNO: 146.4 ± 14.0 s; unpaired *t* test, $p = 0.85$; Fig. 9*E*), open arm (saline: 105.5 ± 10.6 s; CNO: 111.3 ± 11.5 s; unpaired *t* test, $p = 0.71$; Fig. 9*F*), center zone (saline: 43.7 ± 8.3 s; CNO: 38.87 ± 8.1 s; unpaired *t* test, $p = 0.68$; Fig. 9*G*), or total distance traveled (saline: 7.7 ± 0.9 m; CNO: 7.1 ± 1.4 m; unpaired *t* test, $p = 0.69$; Fig. 9*H*). Therefore, activation of hM4Di in dBNST neurons elicits anxiogenic behavior in the EPM in addition to mimicking guanfacine-induced cfos expression.

dBNST activity was monitored via fiber photometry during and before the EPM test (Fig. 10*A*,*B*). GCaMP6f fluorescence signals were normalized to $\Delta F/F_0$ values using segmented normalization and frequencies of Ca^{2+} transients were extracted using the mLspike algorithm (Deneux et al., 2016). To validate the fidelity of Ca^{2+} transient observation by this algorithm, a subset of mice was anesthetized with isoflurane during fiber photometric recordings (Fig. 10*C*). Isoflurane anesthesia decreased dBNST GCaMP6f imputed Ca^{2+} transients from 0.82 ± 0.21 Hz at baseline to 0.06 ± 0.03 Hz (paired *t* test, $p = 0.03$). Having thus validated Ca^{2+} transient quantification, fiber photometric recordings were obtained during a 2 min baseline before the behavioral task and during the 5 min EPM test (Fig. 10*D*). The magnitude of the change in Ca^{2+} transient frequency between the baseline measurements and EPM measurements was calculated (Figs. 10*E*,*F*). In AAV5-hM4Di animals, CNO injection resulted in more Ca^{2+} transients compared with the baseline measurements in the same animal and in saline-injected animals (saline: 2.1 ± 0.6-fold increase; CNO: 6.1 ± 1.6-fold increase; unpaired *t* test, $p = 0.03$; Fig. 10*D*). In AAV5-mCherry controls, CNO injection did not affect this measure (saline: 3.1 ± 0.8-fold increase; CNO: 2.7 ± 0.9-fold increase; unpaired *t* test, $p = 0.75$;

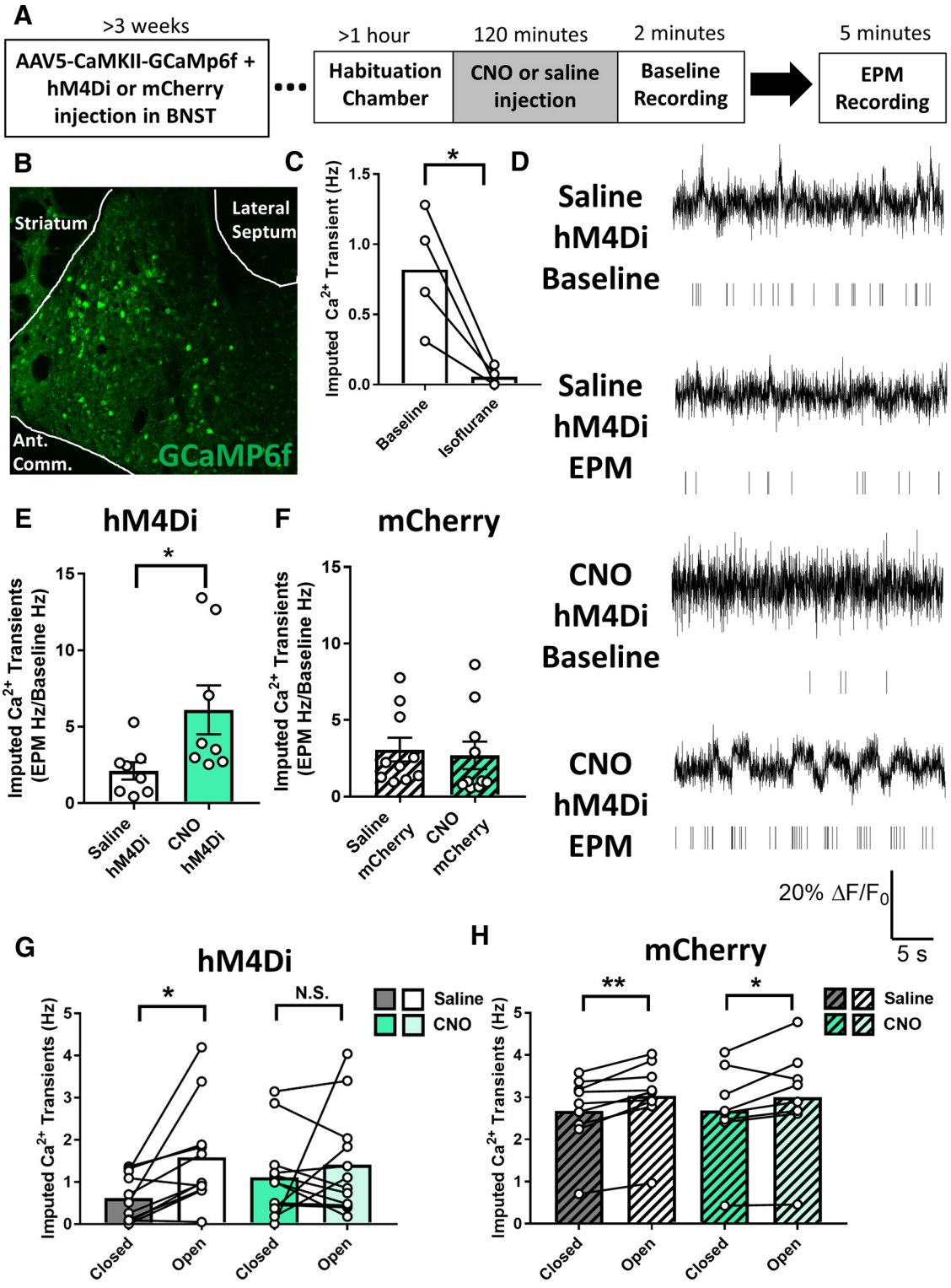

Figure 10. Activation of hM4Di receptors expressed in dBNST neurons elicits GCaMP6f activity increases relative to saline-injected controls. ***A***, Schematic showing the timeline of AAV vector injection, animal habituation, drug injection, baseline fiber photometry recording, and EPM testing. ***B***, Representative image of GCaMP6f expression within the dBNST. ***C***, Imputed Ca^{2+} transients within the dBNST were significantly reduced under isoflurane anesthesia. ***D***, Representative fiber photometry traces showing changes in $\Delta F/F_0$ as a function of time for 2 min after either saline or CNO injection in AAV5-hM4Di animals during baseline recordings or recordings obtained in the EPM. ***E***, Both saline and CNO injections in mice expressing the hM4Di receptor led to an increase in Ca^{2+} transient frequency in the EPM relative to baseline values. The CNO-induced enhancement of activity was greater than that observed in saline-injected animals. ***F***, No differences in the ratio of activity in the EPM relative to baseline were observed between saline- and CNO-injected AAV5-mCherry control animals. ***G***, In saline-injected mice expressing the hM4Di receptor, open arm activity was consistently greater than closed arm activity, as measured by imputed Ca^{2+} transient frequency. In CNO-injected mice expressing the hM4Di receptor, there was no significant difference between the two arms. Repeated-measures two-way ANOVA: EPM arm effect $F_{(1,21)} = 6.32$, $p = 0.02$, CNO effect $F_{(1,21)} = 0.20$, $p = 0.66$, interaction $F_{(1,21)} = 1.78$, $p = 0.20$. ***H***, In both saline- and CNO-injected AAV5-mCherry control mice, open arm activity was greater than closed arm activity. Repeated-measures two-way ANOVA: EPM arm effect $F_{(1,17)} = 20.44$, $p = 0.0003$, CNO effect $F_{(1,17)} = 0.0009$, $p = 0.98$, interaction $F_{(1,17)} = 0.19$, $p = 0.67$. *p*-values were calculated by unpaired *t* test (***C***, ***E***, ***F***) or *post hoc* Holm–Sidak multiple-comparisons test (***G***, ***H***). N,S. $p > 0.05$, $^*p < 0.05$, $^{**}p < 0.01$. $n = 4$–9 animals per group.

Fig. 10*F*). We also assessed dBNST Ca^{2+} transient frequency in relation to mouse location in the maze (Fig. 10*G*). Specifically, a two-way ANOVA showed a significant effect of EPM arm on Ca^{2+} transient frequency ($F_{(1,21)} = 6.32$, $p = 0.02$), but no effect of CNO ($F_{(1,21)} = 0.20$, $p = 0.66$) or interaction between the two ($F_{(1,21)} = 1.78$, $p = 0.20$). A Holm–Sidak multiple-comparisons test showed that saline-injected animals had increased open arm activity relative to closed arm activity (closed arm: 0.6 ± 0.2 Hz; open arm: 1.6 ± 0.4 Hz; $p = 0.03$), but CNO-injected animals did not (closed arm: 1.1 ± 0.3 Hz; open arm: 1.4 ± 0.4 Hz; $p = 0.40$). In AAV5-mCherry controls, a two-way ANOVA also showed a significant effect of EPM arm on Ca^{2+} transient frequency ($F_{(1,17)} = 20.44$, $p = 0.0003$), but no effect of CNO ($F_{(1,17)} = 0.0009$, $p = 0.98$) or an interaction between the two ($F_{(1,17)} = 0.19$, $p = 0.67$). A Holm–Sidak multiple-comparisons test showed that both saline- and CNO-injected animals had increased open arm activity relative to closed arm activity (saline closed arm: 2.2 ± 0.3 Hz, saline open arm: 2.4 ± 0.3 Hz, $p = 0.004$; CNO closed arm: 2.7 ± 0.3 Hz, CNO open arm: 2.9 ± 0.4 Hz, $p = 0.01$; Fig. 10*H*). AAV5-mCherry controls showed higher values of arm-specific BNST Ca^{2+} transient frequency than AAV5-hM4Di experimental animals. However, interpretation of this effect is complicated by potential cohort differences related to signal variability (i.e., viral expression, fiber fidelity), supporting the use of a within-subject experimental design and analysis. Therefore, CNO activation of the hM4Di receptor increases overall Ca^{2+}-signaled activity in the EPM and eliminates the difference of behaving mice between closed and open arm activities.

Discussion

Here, we show that postsynaptic α_{2A}-ARs excite dBNST neurons via HCN channel inhibition, in contrast to presynaptic inhibition. Further, we show that CNO activation of the chemogenetic receptor hM4Di in dBNST neurons mimics aspects of α_{2A}-AR signaling, induces anxiogenesis, and increases *in vivo* neuronal activity. Together, these data inform our understanding of α_{2A}-AR subpopulation interactions and relevance to anxiety and addiction treatments. Moreover, our hM4Di receptor data emphasize that great care must be taken in the interpretation of DREADD-based approaches.

Postsynaptic α_{2A}-ARs mediate guanfacine-induced cfos expression

α_{2A}-ARs are expressed in both presynaptic and postsynaptic compartments throughout the BNST neuronal populations, in addition to glia (Flavin et al., 2014). The functions of these receptor subpopulations are incompletely understood. Within the BNST, α_2-AR agonists inhibit the release of norepinephrine, glutamate, and GABA via presynaptic mechanisms (Palij and Stamford, 1993; Egli et al., 2005; Shields et al., 2009; Krawczyk et al., 2011; Herr et al., 2012). Specificity of presynaptic actions have been shown because guanfacine inhibits afferent-specific stimulation of PBN but not BLA afferents (Flavin et al., 2014). Interestingly, though, in a Thy1-COP4 transgenic mouse line that minimally coexpresses ChR2 with the PBN-marking neuropeptide CGRP, guanfacine enhances ChR2-initiated excitatory transmission (Flavin et al., 2014). This suggests that inhibitory actions at presynaptic α_{2A}-ARs may mask excitatory actions from other receptor subpopulations.

To identify the α_{2A}-AR locus for excitatory actions, we first used voltammetry-validated full- and heteroceptor-specific *Adra2a*$^{-/-}$ mouse lines to differentiate between autoreceptor actions within norepinephrine neurons and heteroceptor actions (Gilsbach et al., 2009). Guanfacine-induced cfos responses were absent in full- and heteroceptor-specific *Adra2a*$^{-/-}$ mice, suggesting that this is a heteroceptor-mediated action, although a ceiling effect could occlude guanfacine actions. Interestingly, full *Adra2a*$^{-/-}$ mice show greater saline injection-induced cfos than WT littermates with intermediate levels in heteroceptor-specific *Adra2a*$^{-/-}$. *Adra2a*$^{-/-}$ mice show baseline anxiety-like behaviors (Schramm et al., 2001; Lähdesmäki et al., 2004) and increased basal immediate early gene expression in stress-sensitive brain regions (Davies et al., 2003). Therefore, we speculate that saline-induced cfos in *Adra2a*$^{-/-}$ mice is stress induced and distinct from guanfacine-induced cfos.

Heteroceptor α_{2A}-ARs are expressed in many cells and locations. We investigated dBNST-expressed α_{2A}-ARs through RNA *in situ* hybridization for the transcript *Adra2a*. *Adra2a*$^{+}$ cells upregulate *Fos* expression after guanfacine relative to saline injection. Like CGRP receptor-expressing neurons in the CeA, *Adra2a*$^{+}$ cells heterogeneously expressed several genetic markers (*Prkcd*, *Penk*, *Calb2*, *Crf*, *Npy*), suggesting that responsivity to catecholamines in *Adra2a*$^{+}$ cells and PBN input in CGRPR^{+} cells define these populations (Han et al., 2015). This shared organization pattern suggests cell-specific informational and functional divergence as a theme of GPCR signaling in the brain. In addition to upregulating *Fos* expression in *Adra2a*$^{+}$ dBNST cells, guanfacine increased the proportion of *Fos*$^{+}$ *Adra2a*$^{-}$ cells, suggesting additional mechanisms underlying guanfacine-induced cfos/*Fos* expression. Disinhibition and/or excitation downstream of *Adra2a*$^{+}$ neurons or network activity outside of the BNST could engage *Adra2a*$^{-}$ dBNST neurons.

Guanfacine initiates cfos expression across the brain (Savchenko and Boughter, 2011). To exclude dBNST neuron activation by network activity, we assessed cfos induction in *ex vivo* brain slices from cfos-eGFP transgenic mice (Barth et al., 2004). Guanfacine incubation recruited cfos-eGFP expression, suggesting sufficiency of α_{2A}-ARs within this simplified system to initiate dBNST cfos expression. Interestingly, *ex vivo* guanfacine-induced cfos expression was larger (4.6-fold increase relative to controls) than *in vivo* (2.8-fold increase), suggesting diminishment by inhibitory circuit activity outside the dBNST.

Multiple α_{2A}-AR agonists induced cfos expression and we also introduced the inhibitory chemogenetic receptor hM4Di into dBNST neurons and observed CNO-induced cfos that mimicked and occluded further guanfacine-induced effects, suggesting translatability among postsynaptic G_i-GPCRs. No cfos activation was observed in controls, confirming hM4Di-specific actions and not off-target effects of CNO or clozapine (Gomez et al., 2017). Although consistent with an intracellular signaling pathway reminiscent of guanfacine-induced cfos expression, the possibility remains that CNO-induced excitatory actions may occur through alternative mechanisms that should be explored in future studies.

Together, this set of convergent data provides strong evidence in support of postsynaptic α_{2A}-ARs inducing cfos expression in a subset of dBNST neurons through a cell-autonomous experience-independent mechanism.

HCN channel involvement in guanfacine-induced activity enhancement

G_i-coupled GPCRs can have excitatory actions through many mechanisms, including alternative adenylyl cyclase recruitment (Federman et al., 1992), augmentation of G_s-coupled GPCR signaling (Andrade, 1993; Winder and Conn, 1993), GPCR-induced channel modulation (Wang et al., 2007), and MAPK/ERK path-

way activation. We tested the hypothesis that α_{2A}-AR-mediated excitation occurs via inhibition of cyclic nucleotide-sensitive HCN channels as occurs in the PFC (Wang et al., 2007). This was based on a high prevalence of HCN-mediated I_h in guanfacine-induced cfos-eGFP$^+$ cells and high *Adra2a* colocalization with *Hcn2*, the HCN subunit with fast kinetics and cAMP sensitivity (Ulens and Tytgat, 2001). Consistent with the proposed mechanism, we show excitatory actions of both α_{2A}-AR agonism and HCN channel inhibition in the Thy1-COP4 mouse line that segregates ChR2 and CGRP expression, although with varying kinetics due to pharmacological differences (Shin et al., 2001).

Further, we assessed HCN inhibition effects on spontaneous excitatory transmission in guanfacine-induced cfos-eGFP$^+$ cells. ZD7288 preincubation increased sEPSP frequency but not amplitude, suggesting an inhibitory role of HCN channels on spontaneous neurotransmission. Although this effect could occur via presynaptic HCN channels, as observed in entorhinal cortex (Huang et al., 2011), we hypothesize that release of filtering at the dendritic spine may uncover previously undetectable synaptic potentials due to small amplitudes and space-clamp error (Larkum et al., 1998; Williams and Mitchell, 2008). Consistent with an HCN channel interaction occurring in dendritic spines, we observed expression of the α_{2A}-AR within this compartment (Flavin et al., 2014). Further, having shown sufficiency of HCN inhibition for excitatory actions, we tested necessity via shRNA-mediated knock-down. Similar to *Adra2a*$^{-/-}$ mice, shHCN1/2-injected animals showed no guanfacine-induced cfos expression but had elevated basal expression, suggesting that reducing HCN-dependent filtering at the dendritic neck releases the inhibitory tone on guanfacine-activated neurons and thus occludes further guanfacine-induced cfos expression. However, shHCN1/2- and GFP-expressing mice did not differ in spontaneous BNST neurotransmission or baseline anxiety-like behaviors. Although one potential explanation of these results is that HCN channel knock-down is sufficient for cfos expression but is insufficient for these effects, confounds related to circuit effects resulting from nonspecific shRNA expression limit interpretability.

Potential anxiogenic actions of G_i-coupled signaling in dBNST neurons

To assess the behavioral relevance of guanfacine-induced activation of dBNST neurons, we investigated CNO effects at dBNST-expressed hM4Di receptors in the EPM. CNO induced anxiogenic behavior (increased closed arm time, decreased open arm time), contrasting with anxiolytic actions of BNST lesions/silencing (Walker et al., 2003). Stress and anxiogenic drug exposure upregulates cfos in the BNST (Cullinan et al., 1995; Singewald et al., 2003), supporting a connection between BNST activation and anxiogenesis. Guanfacine has anxiolytic/antidepressant actions, but with very narrow effective concentrations (Mineur et al., 2015). Our data suggest that the locus of guanfacine anxiolytic/antidepressant actions may be presynaptic.

CNO activation of dBNST-expressed hM4Di receptors enhances neuronal activity in the EPM as measured by GCaMP6f fiber photometry. The profile of activity is treatment dependent because saline-injected animals show higher open arm activity than closed arm activity and CNO-injected animals do not, with saline- or CNO-injected AAV5-mCherry controls resembling saline-injected AAV5-hM4Di animals. Therefore, G_i-coupled GPCR activation in dBNST neurons can be both anxiogenic and activity enhancing within the EPM.

Relevance of hM4Di excitatory actions to the use of DREADDs

In addition to detailing guanfacine effects on dBNST activity, we showed that CNO activation of dBNST-expressed hM4Di is activity enhancing and anxiogenic in the EPM. Neither CNO effect was recapitulated in control animals, highlighting effect specificity. These data question the assumption that hM4Di activation is universally inhibitory, like the assumption that agonism at hM3Dq is universally excitatory that has been confirmed as incomplete (Mazzone et al., 2018). Instead, these data suggest that hM4Di-mediated actions elicit G_i-coupled GPCR signaling cascades that may lead to unexpected cellular responses depending on downstream effectors. This, however, is not surprising given the extant literature on excitatory actions of G_i-GPCRs (Federman et al., 1992; Andrade, 1993; Winder and Conn, 1993; Wang et al., 2007; Kawaura et al., 2014). This highlights the importance of hM4Di effect interpretation as resulting from invoked G_i-GPCR signaling pathways and not necessarily neuronal inhibition.

Limitations and future directions

Clinical studies with guanfacine have begun to uncover potential sex differences (Fox et al., 2014; Milivojevic et al., 2017). For example, guanfacine decreased stress and cue imagery-induced drug craving, anxiety, and negative emotion in cocaine-dependent females but not males (Fox et al., 2014). Similarly, in rodents, guanfacine showed sex differences in cfos expression patterns (Mineur et al., 2015). In the present study, males and females were combined due to lack of apparent sex differences. However, future studies should aim to rigorously test such differences to maximize clinical utility.

Conclusion

Extended amygdala α_{2A}-ARs are targets for anxiety disorders and stress-induced addictive behaviors. Here, we show that postsynaptic α_{2A}-ARs in the dBNST mediated guanfacine-induced cfos expression via an HCN-dependent process. Interestingly, whereas presynaptic α_{2A}-ARs are hypothesized to be anxiolytic, these postsynaptic effects appear to be anxiogenic. Therefore, competition among presynaptic inhibition and postsynaptic excitation may complicate the effects of guanfacine. The interplay among effects at different α_{2A}-AR subpopulations needs to be further explored to support preclinical and clinical approaches to anxiety and addictive disorders.

References

Adhikari A (2014) Distributed circuits underlying anxiety. Front Behav Neurosci 8:112. CrossRef Medline

Andrade R (1993) Enhancement of beta-adrenergic responses by gi-linked receptors in rat hippocampus. Neuron 10:83–88. CrossRef Medline

Arenkiel BR, Peca J, Davison IG, Feliciano C, Deisseroth K, Augustine GJ, Ehlers MD, Feng G (2007) In vivo light induced activation of neural circuitry in transgenic mice expressing channelrhodopsin-2. Neuron 54:205–218. CrossRef Medline

Barth AL, Gerkin RC, Dean KL (2004) Alteration of neuronal firing properties after in vivo experience in a FosGFP transgenic mouse. J Neurosci 24:6466–6475. CrossRef Medline

Blaine SK, Milivojevic V, Fox H, Sinha R (2016) Alcohol effects on stress pathways: impact on craving and relapse risk. Can J Psychiatry 61:145–153. CrossRef Medline

Blaxall HS, Murphy TJ, Baker JC, Ray C, Bylund DB (1991) Characterization of the alpha-2C adrenergic receptor subtype in the opossum kidney and in the OK cell line. J Pharmacol Exp Ther 259:323–329. Medline

Bruijnzeel AW (2017) Neuropeptide systems and new treatments for nicotine addiction. Psychopharmacology 234:1419–1437. CrossRef Medline

Buffalari DM, Baldwin CK, See RE (2012) Treatment of cocaine withdrawal

anxiety with guanfacine: relationships to cocaine intake and reinstatement of cocaine seeking in rats. Psychopharmacology 223:179–190. CrossRef Medline

Conrad KL, Davis AR, Silberman Y, Sheffler DJ, Shields AD, Saleh SA, Sen N, Matthies HJ, Javitch JA, Lindsley CW, Winder DG (2012) Yohimbine depresses excitatory transmission in BNST and impairs extinction of cocaine place preference through orexin-dependent, norepinephrine-independent processes. Neuropsychopharmacology 37:2253–2266. CrossRef Medline

Cui G, Jun SB, Jin X, Pham MD, Vogel SS, Lovinger DM, Costa RM (2013) Concurrent activation of striatal direct and indirect pathways during action initiation. Nature 494:238–242. CrossRef Medline

Cullinan WE, Herman JP, Battaglia DF, Akil H, Watson SJ (1995) Pattern and time course of immediate early gene expression in rat brain following acute stress. Neuroscience 64:477–505. CrossRef Medline

Davies MF, Tsui JY, Flannery JA, Li X, DeLorey TM, Hoffman BB (2003) Augmentation of the noradrenergic system in alpha-2 adrenergic receptor deficient mice: anatomical changes associated with enhanced fear memory. Brain Res 986:157–165. CrossRef Medline

Delfs JM, Zhu Y, Druhan JP, Aston-Jones G (2000) Noradrenaline in the ventral forebrain is critical for opiate withdrawal-induced aversion. Nature 403:430–434. CrossRef Medline

Deneux T, Kaszas A, Szalay G, Katona G, Lakner T, Grinvald A, Rózsa B, Vanzetta I (2016) Accurate spike estimation from noisy calcium signals for ultrafast three-dimensional imaging of large neuronal populations in vivo. Nat Commun 7:12190. CrossRef Medline

Egli RE, Kash TL, Choo K, Savchenko V, Matthews RT, Blakely RD, Winder DG (2005) Norepinephrine modulates glutamatergic transmission in the bed nucleus of the stria terminalis. Neuropsychopharmacology 30:657–668. CrossRef Medline

Erb S, Hitchcott PK, Rajabi H, Mueller D, Shaham Y, Stewart J (2000) Alpha-2 adrenergic receptor agonists block stress-induced reinstatement of cocaine seeking. Neuropsychopharmacology 23:138–150. CrossRef Medline

Federman AD, Conklin BR, Schrader KA, Reed RR, Bourne HR (1992) Hormonal stimulation of adenylyl cyclase through gi-protein beta-gamma subunits. Nature 356:159–161. CrossRef Medline

Flavin SA, Matthews RT, Wang Q, Muly EC, Winder DG (2014) α2A-adrenergic receptors filter parabrachial inputs to the bed nucleus of the stria terminalis. J Neurosci 34:9319–9331. CrossRef Medline

Fox HC, Morgan PT, Sinha R (2014) Sex differences in guanfacine effects on drug craving and stress arousal in cocaine-dependent individuals. Neuropsychopharmacology 39:1527–1537. CrossRef Medline

Gantz SC, Bunzow JR, Williams JT (2013) Spontaneous inhibitory synaptic currents mediated by a g protein-coupled receptor. Neuron 78:807–812. CrossRef Medline

Ghamari-Langroudi M, Digby GJ, Sebag JA, Millhauser GL, Palomino R, Matthews R, Gillyard T, Panaro BL, Tough IR, Cox HM, Denton JS, Cone RD (2015) G-protein-independent coupling of MC4R to Kir7.1 in hypothalamic neurons. Nature 520:94–98. CrossRef Medline

Gilsbach R, Röser C, Beetz N, Brede M, Hadamek K, Haubold M, Leemhuis J, Philipp M, Schneider J, Urbanski M, Szabo B, Weinshenker D, Hein L (2009) Genetic dissection of alpha2-adrenoceptor functions in adrenergic versus nonadrenergic cells. Mol Pharmacol 75:1160–1170. CrossRef Medline

Goeders NE (2003) The impact of stress on addiction. Eur Eur Neuropsychopharmacol 13:435–441. CrossRef Medline

Gomez JL, Bonaventura J, Lesniak W, Mathews WB, Sysa-Shah P, Rodriguez LA, Ellis RJ, Richie CT, Harvey BK, Dannals RF, Pomper MG, Bonci A, Michaelides M (2017) Chemogenetics revealed: DREADD occupancy and activation via converted clozapine. Science 357:503–507. CrossRef Medline

Griebel G, Holmes A (2013) 50 years of hurdles and hope in anxiolytic drug discovery. Nat Rev Drug Discov 12:667–687. CrossRef Medline

Han S, Soleiman M, Soden ME, Zweifel LS, Palmiter RD (2015) Elucidating an affective pain circuit that creates a threat memory. Cell 162:363–374. CrossRef Medline

Heilig M, Egli M (2006) Pharmacological treatment of alcohol dependence: target symptoms and target mechanisms. Pharmacol Ther 111:855–876. CrossRef Medline

Heilig M, Egli M, Crabbe JC, Becker HC (2010) Acute withdrawal, protracted abstinence and negative affect in alcoholism: are they linked? Addict. CrossRef Medline

Herr NR, Park J, McElligott ZA, Belle AM, Carelli RM, Wightman RM (2012) In vivo voltammetry monitoring of electrically evoked extracellular norepinephrine in subregions of the bed nucleus of the stria terminalis. J Neurophysiol 107:1731–1737. CrossRef Medline

Highfield D, Yap J, Grimm JW, Shalev U, Shaham Y (2001) Repeated lofexidine treatment attenuates stress-induced, but not drug cues-induced reinstatement of a heroin-cocaine mixture (speedball) seeking in rats. Neuropsychopharmacology 25:320–331. CrossRef Medline

Holleran KM, Wilson HH, Fetterly TL, Bluett RJ, Centanni SW, Gilfarb RA, Rocco LE, Patel S, Winder DG (2016) Ketamine and MAG lipase inhibitor-dependent reversal of evolving depressive-like behavior during forced abstinence from alcohol drinking. Neuropsychopharmacology 41:2062–2071. CrossRef Medline

Huang Z, Lujan R, Kadurin I, Uebele VN, Renger JJ, Dolphin AC, Shah MM (2011) Presynaptic HCN1 channels regulate Cav3.2 activity and neurotransmission at select cortical synapses. Nat Neurosci 14:478–486. CrossRef Medline

Jasper JR, Lesnick JD, Chang LK, Yamanishi SS, Chang TK, Hsu SA, Daunt DA, Bonhaus DW, Eglen RM (1998) Ligand efficacy and potency at recombinant alpha2 adrenergic receptors: agonist-mediated [35S]GTPgammaS binding. Biochem Pharmacol 55:1035–1043. CrossRef Medline

Ji MH, Jia M, Zhang MQ, Liu WX, Xie ZC, Wang ZY, Yang JJ (2014) Dexmedetomidine alleviates anxiety-like behaviors and cognitive impairments in a rat model of post-traumatic stress disorder. Prog Neuropsychopharmacol Biol Psychiatry 54:284–288. CrossRef Medline

Kash TL, Winder DG (2006) Neuropeptide Y and corticotropin-releasing factor bi-directionally modulate inhibitory synaptic transmission in the bed nucleus of the stria terminalis. Neuropharmacology 51:1013–1022. CrossRef Medline

Kassel JD, Stroud LR, Paronis CA (2003) Smoking, stress, and negative affect: correlation, causation, and context across stages of smoking. Psychol Bull 129:270–304. CrossRef Medline

Kawaura K, Karasawa J, Chaki S, Hikichi H (2014) Stimulation of postsynapse adrenergic alpha2A receptor improves attention/cognition performance in an animal model of attention deficit hyperactivity disorder. Behav Brain Res 270:349–356. CrossRef Medline

Kessler RC, Berglund P, Demler O, Jin R, Merikangas KR, Walters EE (2005) Lifetime prevalence and age-of-onset distributions of DSM-IV disorders in the national comorbidity survey replication set distributions of DSM-IV disorders in the national comorbidity survey replication. Arch Gen Psychiatry 62:593–602. CrossRef Medline

Koob GF (2009) Brain stress systems in the amygdala and addiction. Brain Res 1293:61–75. CrossRef Medline

Krawczyk M, Georges F, Sharma R, Mason X, Berthet A, Bézard E, Dumont EC, Bezard E, Dumont ÉC, Bezard E, Dumont EC, Bézard E, Dumont EC (2011) Double-dissociation of the catecholaminergic modulation of synaptic transmission in the oval bed nucleus of the stria terminalis. J Neurophysiol 105:145–153. CrossRef Medline

Kupferschmidt DA, Cody PA, Lovinger DM, Davis MI (2015) Brain BLAQ: post-hoc thick-section histochemistry for localizing optogenetic constructs in neurons and their distal terminals. Front Neuroanat 9:6. CrossRef Medline

Kupferschmidt DA, Juczewski K, Cui G, Johnson KA, Lovinger DM (2017) Parallel, but dissociable, processing in discrete corticostriatal inputs encodes skill learning. Neuron 96:476–489.e5. CrossRef Medline

Lähdesmäki J, Sallinen J, MacDonald E, Kobilka BK, Fagerholm V, Scheinin M (2002) Behavioral and neurochemical characterization of alpha2A-adrenergic receptor knockout mice. Neuroscience 113:289–299. CrossRef Medline

Lähdesmäki J, Sallinen J, MacDonald E, Scheinin M (2004) Alpha2A-adrenoceptors are important modulators of the effects of D-amphetamine on startle reactivity and brain monoamines. Neuropsychopharmacology 29:1282–1293. CrossRef Medline

Lampert R, Tuit K, Hong KI, Donovan T, Lee F, Sinha R (2016) Cumulative stress and autonomic dysregulation in a community sample. Stress 19:269–279. CrossRef Medline

Larkum ME, Launey T, Dityatev A, Lüscher HR (1998) Integration of excitatory postsynaptic potentials in dendrites of motoneurons of rat spinal cord slice cultures. J Neurophysiol 80:924–935. CrossRef Medline

Larzelere MM, Jones GN (2008) Stress and health. Prim Care 35:839–856. CrossRef Medline

MacLennan SJ, Luong LA, Jasper JR, To ZP, Eglen RM (1997) Characterization of α2-adrenoceptors mediating contraction of dog saphenous vein: identity with the human α(2A) subtype. Br J Pharmacol 121:1721–1729. CrossRef Medline

Mantsch JR, Weyer A, Vranjkovic O, Beyer CE, Baker DA, Caretta H (2010) Involvement of noradrenergic neurotransmission in the stress- but not cocaine-induced reinstatement of extinguished cocaine-induced conditioned place preference in mice: role for β-2 adrenergic receptors. Neuropsychopharmacology 35:2165–2178. CrossRef Medline

Mazzone CM, Pati D, Michaelides M, DiBerto J, Fox JH, Tipton G, Anderson C, Duffy K, McKlveen JM, Hardaway JA, Magness ST, Falls WA, Hammack SE, McElligott ZA, Hurd YL, Kash TL (2018) Acute engagement of gq-mediated signaling in the bed nucleus of the stria terminalis induces anxiety-like behavior. Mol Psychiatry 23:143–153. CrossRef Medline

McEwen BS (2004) Protection and damage from acute and chronic stress: allostasis and allostatic overload and relevance to the pathophysiology of psychiatric disorders. Ann N Y Acad Sci 1032:1–7. CrossRef Medline

Melchior JR, Jones SR (2017) Chronic ethanol exposure increases inhibition of optically targeted phasic dopamine release in the nucleus accumbens core and medial shell ex vivo. Mol Cell Neurosci 85:93–104. CrossRef Medline

Melchior JR, Ferris MJ, Stuber GD, Riddle DR, Jones SR (2015) Optogenetic versus electrical stimulation of dopamine terminals in the nucleus accumbens reveals local modulation of presynaptic release. J Neurochem 134: 833–844. CrossRef Medline

Milivojevic V, Fox HC, Jayaram-Lindstrom N, Hermes G, Sinha R (2017) Sex differences in guanfacine effects on stress-induced stroop performance in cocaine dependence. Drug Alcohol Depend 179:275–279. CrossRef Medline

Miloyan B, Joseph Bienvenu O, Brilot B, Eaton WW (2018) Adverse life events and the onset of anxiety disorders. Psychiatry Res 259:488–492. CrossRef Medline

Mineur YS, Bentham MP, Zhou WL, Plantenga ME, McKee SA, Picciotto MR (2015) Antidepressant-like effects of guanfacine and sex-specific differences in effects on c-fos immunoreactivity and paired-pulse ratio in male and female mice. Psychopharmacology 232:3539–3549. CrossRef Medline

Nicholas AP, Pieribone V, Hökfelt T (1993) Distributions of mRNAs for alpha-2 adrenergic receptor subtypes in rat brain: an in situ hybridization study. J Comp Neurol 328:575–594. CrossRef Medline

Olsen CM, Winder DG (2010) Operant sensation seeking in the mouse. J Vis Exp 45:2292. CrossRef Medline

Palij P, Stamford JA (1993) Real-time monitoring of endogenous noradrenaline release in rat brain slices using fast cyclic voltammetry. 2. Operational characteristics of the alpha 2 autoreceptor in the bed nucleus of stria terminalis, pars ventralis. Brain Res 607:134–140. CrossRef Medline

Park J, Kile BM, Wightman RM (2009) In vivo voltammetric monitoring of norepinephrine release in the rat ventral bed nucleus of the stria terminalis and anteroventral thalamic nucleus. Eur J Neurosci 30:2121–2133. CrossRef Medline

Paxinos G, Franklin B (2004) The mouse brain in stereotaxic coordinates, 3rd edition. Cambridge, Massachusetts: Academic Press.

Savchenko VL, Boughter JD Jr (2011) Regulation of neuronal activation by alpha2A adrenergic receptor agonist. Neurotox Res 20:226–239. CrossRef Medline

Schramm NL, McDonald MP, Limbird LE (2001) The alpha(2a)-adrenergic receptor plays a protective role in mouse behavioral models of depression and anxiety. J Neurosci 21:4875–4882. CrossRef Medline

Schweimer J, Fendt M, Schnitzler HU (2005) Effects of clonidine injections into the bed nucleus of the stria terminalis on fear and anxiety behavior in rats. Eur J Pharmacol 507:117–124. CrossRef Medline

Shaham Y, Highfield D, Delfs J, Leung S, Stewart J (2000) Clonidine blocks stress-induced reinstatement of heroin seeking in rats: an effect independent of locus coeruleus noradrenergic neurons. Eur J Neurosci 12:292–302. CrossRef Medline

Shalev U, Morales M, Hope B, Yap J, Shaham Y (2001) Time-dependent changes in extinction behavior and stress-induced reinstatement of drug seeking following withdrawal from heroin in rats. Psychopharmacology 156:98–107. CrossRef Medline

Sharma S, Powers A, Bradley B, Ressler KJ (2016) Gene × environment determinants of stress- and anxiety-related disorders. Annu Rev Psychol 67:239–261. CrossRef Medline

Shields AD, Wang Q, Winder DG (2009) alpha2A-adrenergic receptors heterosynaptically regulate glutamatergic transmission in the bed nucleus of the stria terminalis. Neuroscience 163:339–351. CrossRef Medline

Shin KS, Rothberg BS, Yellen G (2001) Blocker state dependence and trapping in hyperpolarization-activated cation channels: evidence for an intracellular activation gate. J Gen Physiol 117:91–101. CrossRef Medline

Silberman Y, Matthews RT, Winder DG (2013) A corticotropin releasing factor pathway for ethanol regulation of the ventral tegmental area in the bed nucleus of of the stria terminalis. J Neurosci 33:950–960. CrossRef Medline

Singewald N, Salchner P, Sharp T (2003) Induction of c-fos expression in specific areas of the fear circuitry in rat forebrain by anxiogenic drugs. Biol Psychiatry 53:275–283. CrossRef Medline

Sinha R, Catapano D, O'Malley S (1999) Stress-induced craving and stress response in cocaine dependent individuals. Psychopharmacology 142: 343–351. CrossRef Medline

Sinha R, Shaham Y, Heilig M (2011) Translational and reverse translational research on the role of stress in drug craving and relapse. Psychopharmacology 218:69–82. CrossRef Medline

Stein MB, Sareen J (2015) Generalized anxiety disorder. N Engl J Med 373: 2059–2068. CrossRef Medline

Strawn JR, Compton SN, Robertson B, Albano AM, Hamdani M, Rynn MA (2017) Extended release guanfacine in pediatric anxiety disorders: a pilot, randomized, placebo-controlled trial. J Child Adolesc Psychopharmacol 27:29–37. CrossRef Medline

Ulens C, Tytgat J (2001) Functional heteromerization of HCN1 and HCN2 pacemaker channels. J Biol Chem 276:6069–6072. CrossRef Medline

Vacher B, Funes P, Chopin P, Cussac D, Heusler P, Tourette A, Marien M (2010) Rigid analogues of the α2-adrenergic blocker atipamezole: small changes, big consequences. J Med Chem 53:6986–6995. CrossRef Medline

Vucicevic J, Srdic-Rajic T, Pieroni M, Laurila JM, Perovic V, Tassini S, Azzali E, Costantino G, Glisic S, Agbaba D, Scheinin M, Nikolic K, Radi M, Veljkovic N (2016) A combined ligand- and structure-based approach for the identification of rilmenidine-derived compounds which synergize the antitumor effects of doxorubicin. Bioorg Med Chem 24:3174–3183. CrossRef Medline

Wahl-Schott C, Biel M (2009) HCN channels: structure, cellular regulation and physiological function. Cell Mol Life Sci 66:470–494. CrossRef Medline

Walker DL, Toufexis DJ, Davis M (2003) Role of the bed nucleus of the stria terminalis versus the amygdala in fear, stress, and anxiety. Eur J Pharmacol 463:199–216. CrossRef Medline

Wang M, Ramos BP, Paspalas CD, Shu Y, Simen A, Duque A, Vijayraghavan S, Brennan A, Dudley A, Nou E, Mazer J a, McCormick DA, Arnsten AF (2007) Alpha2A-adrenoceptors strengthen working memory networks by inhibiting cAMP-HCN channel signaling in prefrontal cortex. Cell 129:397–410. CrossRef Medline

Wang X, Cen X, Lu L (2001) Noradrenaline in the bed nucleus of the stria terminalis is critical for stress-induced reactivation of morphine-conditioned place preference in rats. Eur J Pharmacol 432:153–161. CrossRef Medline

Weitlauf C, Egli RE, Grueter BA, Winder DG (2004) High-frequency stimulation induces ethanol-sensitive long-term potentiation at glutamatergic synapses in the dorsolateral bed nucleus of the stria terminalis. J Neurosci 24:5741–5747. CrossRef Medline

Wightman RM, Amatore C, Engstrom RC, Hale PD, Kristensen EW, Kuhr WG, May LJ (1988) Real-time characterization of dopamine overflow and uptake in the rat striatum. Neuroscience 25:513–523. CrossRef Medline

Williams SR, Mitchell SJ (2008) Direct measurement of somatic voltage clamp errors in central neurons. Nat Neurosci 11:790–798. CrossRef Medline

Wills TA, Klug JR, Silberman Y, Baucum AJ, Weitlauf C, Colbran RJ, Delpire E, Winder DG (2012) GluN2B subunit deletion reveals key role in acute and chronic ethanol sensitivity of glutamate synapses in bed nucleus of the stria terminalis. Proc Natl Acad Sci U S A 109:E278–E287. CrossRef Medline

Winder DG, Conn PJ (1993) Activation of metabotropic glutamate receptors increases cAMP accumulation in hippocampus by potentiating responses to endogenous adenosine. J Neurosci 13:38–44. CrossRef Medline